

RKPM Approach to Elastic-Plastic Fracture Mechanics with Notes on Particles Distribution and Discontinuity Criteria

Mohammad Mashayekhi¹, Hossein M. Shodja^{1,2} and Reza Namakian¹

Abstract: A meshless method called reproducing kernel particle method (RKPM) is exploited to cope with elastic-plastic fracture mechanics (EPFM) problems. The idea of arithmetic progression is assumed to place particles within the refinement zone in the vicinity of the crack tip. A comparison between two conventional treatments, visibility and diffraction, to crack discontinuity is conducted. Also, a tracking to find the appropriate diffraction parameter is performed. To assess the suggestions made, two mode I numerical simulations, pure tension and pure bending tests, are executed. Results including J integral, crack mouth opening displacement (CMOD), and plastic zone size and shape are compared with finite element method (FEM).

Keywords: Meshless, Reproducing kernel particle method (RKPM), Elastic-plastic fracture mechanics (EPFM), Progression, Visibility, Diffraction, J integral, Crack mouth opening displacement (CMOD), Plastic zone.

1 Introduction

Recently, meshless methods, such as element-free Galerkin method (EFGM) [Belytschko, Lu, and Gu (1994) and Lu, Belytschko, and Gu (1994)], reproducing kernel particle method (RKPM) [Liu, Jun, and Zhang (1995) and Liu, Chen, Uras, and Chang (1996)], local boundary integral equation (LBIE) [Zhu, Zhang, and Atluri (1998)], meshless local Petrov-Galerkin (MLPG) [Zhu, Zhang, and Atluri (1998), Atluri, Kim, and Cho (1999), Atluri and Shen (2002), and Atluri (2004)], and gradient reproducing kernel particle method (GRKPM) [Shodja and Hashemian (2007, 2008) and Hashemian and Shodja (2008a, b)], are increasingly utilized in solving

¹ Center of Excellence in Structures and Earthquake Engineering, Department of Civil Engineering, Sharif University of Technology, P. O. Box 11155-9313, Tehran, Iran

² Institute for Nanoscience and Nanotechnology, Sharif University of Technology, P. O. Box, 11155-9161, Tehran, Iran

various types of boundary value problems which are described by some partial differential equations along with some appropriate boundary conditions. This is due to the capability of these methods in providing smooth approximations up to the desirable order, and in contrast with finite element method (FEM) in which meshing the entire domain with presumed connectivity is necessary, can be implemented more efficiently and conveniently, particularly for problems with complex geometries. Some valuable overviews have been presented by [Belytschko, Krongauz, Organ, Fleming, and Krysl (1996)] and [Nguyen, Rabczuk, Bordas, and DufLOT (2008)]. A unified approach to the mathematical analysis of such meshless approaches as generalized RKPM, GRKPM, and generalized moving least square (GMLS) [Behzadan, Shodja, and Khezri (2010)] has been recently presented. In the current article, RKPM is adopted due to possessing appropriate features for satisfying the consistency conditions [Jin, Li, and Aluru (2001)], specifically over boundaries [Liu, Jun, and Zhang (1995)].

Throughout numerical analyses of fracture mechanics problems, the concept of energy release rate, first introduced by [Cherepanov (1967)] and [Eshelby (1970)], is often used which results in achieving almost accurate characterization of the domain of solution. [Rice (1968)] presented this concept by means of J integral. It can be shown that in linear elastic fracture mechanics (LEFM) J has a direct relationship with the stress intensity factors (SIFs). Also, in nonlinear fracture mechanics, [Hutchinson (1968)] and [Rice and Rosengren (1968)] by assuming deformation plasticity and planar conditions (plane strain and plane stress), presented a relationship in the vicinity of the crack tip for displacement, strain, and stress fields, known as HRR singular fields, and showed that the amplitudes of these fields can be expressed in terms of J integral. [Rao and Rahman (2004)] by approximating HRR fields introduced enriched bases, which span these approximating fields in element free Galerkin method (EFGM). However, it must be noted that, enriched basis functions, used in EFGM cannot necessarily be reproduced exactly via RKPM [Liu, Li, and Belytschko (1997)]. Since HRR is based on deformation plasticity, it requires that unloading does not occur at any point within the medium under consideration. But, it should be noted that even with monotonically increasing applied loading, there is no guarantee that local unloading would not occur [Anderson (1995)]. To circumvent this shortcoming, incremental plasticity that gives a more realistic description of elastic-plastic behavior of ductile materials is adopted; however, in the context of this theory J integral loses its path independent property. In such situation, [Yuan and Brocks (1991)] and Simha and his colleagues [Simha, Fischer, Shan, Chen, and Kolednik (2008)] have shown that the far-field real or saturated J value attained through incremental plasticity for contained yielding has a good agreement with the results achieved based on deformation plasticity as well as ex-

periment's.

There have been two widely used treatments, namely visibility and diffraction for dealing with the internal discontinuity in fracture mechanics [Belytschko, Lu, and Gu L (1994), Krysl and Belytschko (1996), Organ, Fleming, Terry, and Belytschko (1996), and Belytschko, Krongauz, Organ, Fleming, and Krysl (1996)]. To date, no investigation on their ability in handling elastic-plastic fracture mechanics (EPFM) problems has been yet presented, while selecting the appropriate treatment may affect the solution drastically. Furthermore, for those situations where diffraction method is recommended some suggestions are made about its parameter [Organ, Fleming, Terry, and Belytschko (1996), Belytschko (1997)] without any parametric study.

The main objective of the present work is to make certain recommendations for enhancing the accuracy of RKPM approximation applied to EPFM problems. The recommended techniques take advantage of the inherent features of RKPM, and considers just polynomials in the basis functions. After a quick description of RKPM, weak form of nonlinear equilibrium equation, and incremental plasticity relationships, the progression idea in placing particles around the crack tip and treatment to crack discontinuity are presented. A brief overview on J integral will be given. In the section on numerical results, the effect of the progression technique is investigated. Afterwards, by utilizing the best refinement deduced from the first set of experiments, the performances of visibility and diffraction methods in modeling the crack discontinuity in EPFM problems are assessed. Subsequently, a tracking for diffraction parameter is performed. Finally, with the best combination of refinement and appropriate discontinuity treatment, for two cases of increasing tensile and bending far-field stresses applied to a cracked plate, J integral, crack mouth opening displacement (CMOD), and the crack-tip plastic zone size and shape are computed and compared with the results obtained using FEM.

2 Two-dimensional RKPM

Through this work, in-plane problems are examined. For self-containment and convenience of presenting the formulation of EPFM in the framework of RKPM, 2D RKPM is briefly reviewed in this section.

2.1 Reproducing equation

In the conventional RKPM, a scalar function $u(\mathbf{x})$ can be expressed by the following reproducing formula

$$u^R(\mathbf{x}) = \int_{\Gamma} u(\mathbf{y}) \bar{\phi}_p(\mathbf{x}; \mathbf{x} - \mathbf{y}) d\mathbf{y}, \quad (1)$$

in which the bold face variables \mathbf{y} and \mathbf{x} are the field points, $u^R(\mathbf{x})$ is the reproduced function, ρ is the dilation parameter, and $\bar{\phi}_\rho(\mathbf{x}; \mathbf{x} - \mathbf{y})$ is the modified kernel function that is defined by

$$\bar{\phi}_\rho(\mathbf{x}; \mathbf{x} - \mathbf{y}) = C(\mathbf{x}; \mathbf{x} - \mathbf{y}) \phi_\rho(\mathbf{x} - \mathbf{y}), \quad (2)$$

where $C(\mathbf{x}; \mathbf{x} - \mathbf{y})$ is the correction function [Liu, Jun, and Zhang (1995)]

$$C(\mathbf{x}; \mathbf{x} - \mathbf{y}) = \mathbf{P}^T(\mathbf{x} - \mathbf{y}) \boldsymbol{\beta}(\mathbf{x}), \quad (3)$$

and $\phi_\rho(\mathbf{x} - \mathbf{y})$ is the window function. For a 2D domain, the vector of independent basis functions, $\mathbf{P}(\mathbf{x} - \mathbf{y})$, and the vector of unknown coefficients, $\boldsymbol{\beta}(\mathbf{x})$, are defined as follows

$$\begin{aligned} \mathbf{P}^T(\mathbf{x} - \mathbf{y}) \\ = [1 \quad x_1 - y_1 \quad x_2 - y_2 \quad (x_1 - y_1)^2 \quad (x_1 - y_1)(x_2 - y_2) \quad (x_2 - y_2)^2 \quad \dots], \end{aligned} \quad (4)$$

and

$$\boldsymbol{\beta}^T(\mathbf{x}) = [\beta_{00} \quad \beta_{10} \quad \beta_{01} \quad \beta_{20} \quad \beta_{11} \quad \beta_{02} \quad \dots], \quad (5)$$

respectively.

2.2 Completeness

2.2.1 Conditions on the function

Consider the Taylor series expansion of u about point \mathbf{x}

$$u(\mathbf{y}) = u(\mathbf{x}) - \int_{i=1}^2 (x_i - y_i) \frac{\partial u(\mathbf{x})}{\partial x_i} + \frac{1}{2!} \int_{i=1}^2 \int_{j=1}^2 (x_i - y_i)(x_j - y_j) \frac{\partial^2 u(\mathbf{x})}{\partial x_i \partial x_j} + \dots \quad (6)$$

By substituting Eq. (6) into (1), one can obtain

$$\begin{aligned} u^R(\mathbf{x}) = \bar{m}_{00}(\mathbf{x}) u(\mathbf{x}) - \bar{m}_{10}(\mathbf{x}) \frac{\partial u(\mathbf{x})}{\partial x_1} - \bar{m}_{01}(\mathbf{x}) \frac{\partial u(\mathbf{x})}{\partial x_2} + \frac{1}{2} \bar{m}_{20}(\mathbf{x}) \frac{\partial^2 u(\mathbf{x})}{\partial x_1^2} \\ + \bar{m}_{11}(\mathbf{x}) \frac{\partial^2 u(\mathbf{x})}{\partial x_1 \partial x_2} + \frac{1}{2} \bar{m}_{02}(\mathbf{x}) \frac{\partial^2 u(\mathbf{x})}{\partial x_2^2} + \dots, \end{aligned} \quad (7)$$

where $\bar{m}_{\alpha_1 \alpha_2}(\mathbf{x})$ is the moment of the corrected window function defined as

$$\bar{m}_{\alpha_1 \alpha_2}(\mathbf{x}) = \int_{\Omega} (x_1 - y_1)^{\alpha_1} (x_2 - y_2)^{\alpha_2} \bar{\phi}_\rho(\mathbf{x}; \mathbf{x} - \mathbf{y}) d\mathbf{y}. \quad (8)$$

2.3 RKPM shape functions and their derivatives

2.3.1 The shape functions

On account of the computational aims, the continuous integrals in expressions (1) and (12) should be discretized. To satisfy the consistency conditions same discretization rule must be utilized for both integrals. Using trapezoidal rule and considering (1), (2), and (3) one can conclude

$$u^R(\mathbf{x}) = \int_{I=1}^{NP} \psi^I(\mathbf{x}) \hat{u}^I, \quad (15)$$

where NP is the number of particles distributed throughout the domain Ω , \hat{u}^I is called the (horizontal) fictitious nodal value pertinent to the I th particle[Zhu, Atluri (1998)], and

$$\psi^I(\mathbf{x}) = \mathbf{P}^T(\mathbf{x} - \mathbf{x}^I) \boldsymbol{\beta}(\mathbf{x}) \phi_\rho(\mathbf{x} - \mathbf{x}^I) \Delta S^I, \quad (16)$$

where $\psi^I(\mathbf{x})$ and ΔS^I are the shape function and the area in 2D case associated with the I th particle, respectively. The computation of ΔS^I will be described in section 2.5.

2.3.2 Derivatives of the shape functions

By considering (15) and deriving from the Eq. (16) with respect to x_k , the definition of the derivative of the I th shape function becomes [Liu, Chen, Uras, and Chang (1996)]

$$\begin{aligned} \psi_{,x_k}^I(\mathbf{x}) = & \left[\mathbf{P}_{,x_k}^T(\mathbf{x} - \mathbf{x}^I) \boldsymbol{\beta}(\mathbf{x}) \phi_\rho(\mathbf{x} - \mathbf{x}^I) \right. \\ & \left. + \mathbf{P}^T(\mathbf{x} - \mathbf{x}^I) \boldsymbol{\beta}_{,x_k}(\mathbf{x}) \phi_\rho(\mathbf{x} - \mathbf{x}^I) + \mathbf{P}^T(\mathbf{x} - \mathbf{x}^I) \boldsymbol{\beta}(\mathbf{x}) \phi_{\rho,x_k}(\mathbf{x} - \mathbf{x}^I) \right] \Delta S^I. \end{aligned} \quad (17)$$

To attain the derivatives of the shape functions, the values of unknown coefficients $\boldsymbol{\beta}(\mathbf{x})$ and $\boldsymbol{\beta}_{,x_k}(\mathbf{x})$ calculated from (14) must be substituted into (17).

2.4 Selection of the basis and the window function

In this work, the linear basis $\mathbf{P}^T(\mathbf{x} - \mathbf{y}) = [1 \quad x_1 - y_1 \quad x_2 - y_2]$ which is proved to be a good trade-off between speed and accuracy to reach the highest efficiency is chosen. There are various window functions having been used in the literature [Belytschko, Lu, and Gu (1994), Lu, Belytschko, Gu (1994), Liu and Chen (1995), and Liu (2003)]. Since, current work deals with the equilibrium equation, its weak

form urges the selected window function and its first derivatives to be continuous. Hence, Gaussian function is used

$$\phi(d_I) = \begin{cases} \frac{e^{-(d_I/c_I)^2} - e^{-(\rho_I/c_I)^2}}{1 - e^{-(\rho_I/c_I)^2}}, & d_I \leq \rho_I, \\ 0, & d_I > \rho_I, \end{cases} \quad (18)$$

where $d_I(\mathbf{x}) = \mathbf{x} - \mathbf{x}^I$ is the distance between the I th particle and a sampling point \mathbf{x} , ρ_I is the dilation parameter, and c_I is a parameter controlling the effective domain of influence of I th particle. c_I and ρ_I are defined by

$$c_I = \eta c^I, \quad \rho_I = \rho_{max} c^I, \quad (19)$$

in which ρ_{max} and η are constants and should be chosen in such way that $\rho_{max}/\eta \geq 4.0$ is satisfied to avoid singular moment matrix [Belytschko (1997)]. To retain smooth shape functions and to treat high gradient problem with more accuracy $\eta \approx 1$ is recommended [Lu, Belytschko, Gu (1994)]. Also, the weight function parameter $\rho_{max} = 4$ is used. c^I is a characteristic nodal spacing which for a regular array of particles is assumed the distance from the I th particle to the second nearest particle, and for a irregular array is the distance to the fourth nearest one. Also, $\phi_p(d_I)$ is defined

$$\phi_p(d_I) = \frac{\kappa}{\rho_I^2} \phi(d_I), \quad (20)$$

in which κ is the normalizing factor [Li and Liu (2004)] where for the Gaussian window function mentioned in Eq. (18) becomes

$$\kappa = \frac{1}{\left(\frac{1}{\left(\frac{\rho_{max}}{\eta}\right)^2} + \frac{1}{1 - e^{\left(\frac{\rho_{max}}{\eta}\right)^2}} \right)}. \quad (21)$$

2.5 Determining the particle volume

One of the effectual parameters considered in RKPM rather than EFGM is the volume pertinent to each particle, ΔS^I , which is one of its characteristics. In the case of regular distribution of particles, the calculation of their volumes is a straightforward task. However, when the arrangement of particles is non-uniform, the procedure of finding an appropriate particle volume comes to be cumbersome. To this end, an efficient computational algorithm has been proposed by [Khezri, Hashemian, and Shodja (2009)], in which the entire domain of a 2D problem is discretized with a very fine mesh. Each cell in this mesh represents a point in the domain. Afterwards,

the volume of each particle that is its area in a 2D problem comprises the areas of cells whose representative points are closer to the current particle than the others. In addition, in the corresponding article a systematic procedure fitting computer programming has been put forward.

3 Weak form and discretization

The equilibrium equation within a 2D medium, Ω , is given by

$$\nabla \cdot \boldsymbol{\sigma} + \mathbf{b} = \mathbf{0} \quad \text{in } \Omega. \quad (22)$$

Also, the natural and essential boundary conditions are

$$\boldsymbol{\sigma} \cdot \mathbf{n} = \bar{\mathbf{t}} \quad \text{on } \Gamma_t, \quad \mathbf{u} = \bar{\mathbf{u}} \quad \text{on } \Gamma_u, \quad (23)$$

respectively, where $\boldsymbol{\sigma}$, \mathbf{u} , and \mathbf{b} are the stress tensor, displacement and body force vectors, respectively. $\bar{\mathbf{t}}$ is the prescribed traction on Γ_t , and also, $\bar{\mathbf{u}}$ is the displacement vector on Γ_u . \mathbf{n} is the unit normal to the domain.

3.1 Weak form

The weak form of (22) via weighted residual method is

$$\int_{\Omega} \delta \boldsymbol{\varepsilon}^T \boldsymbol{\sigma} d\Omega - \int_{\Omega} \delta \mathbf{u}^T \mathbf{b} d\Omega - \int_{\Gamma_t} \delta \mathbf{u}^T \bar{\mathbf{t}} d\Gamma + \delta W_u = 0, \quad (24)$$

where δ represents the variational operator. For plane strain condition in the vector form we have

$$\boldsymbol{\sigma}^T = [\sigma_{11} \quad \sigma_{22} \quad \tau_{12}], \quad \boldsymbol{\varepsilon}^T = [\varepsilon_{11} \quad \varepsilon_{22} \quad \gamma_{12}], \quad \mathbf{u}^T = [u_1 \quad u_2]. \quad (25)$$

The term required to enforce the essential boundary conditions via penalty method [Zhu and Atluri (1998)] together with its variational form are

$$W_u = \frac{\beta}{2} \int_{\Gamma_u} (\mathbf{u} - \bar{\mathbf{u}})^T (\mathbf{u} - \bar{\mathbf{u}}) d\Gamma, \quad \delta W_u = \beta \int_{\Gamma_u} \delta \mathbf{u}^T (\mathbf{u} - \bar{\mathbf{u}}) d\Gamma. \quad (26)$$

in which β is the penalty coefficient. Since the stress-strain relationship in plastic state is non-linear, Eq. (24) is also non-linear with respect to the displacement \mathbf{u} . In order to solve Eq. (24), the standard Newton-Raphson method is employed; so, it should be linearized as follows

$$\begin{aligned} \int_{\Omega} \delta \boldsymbol{\varepsilon}^T \mathbf{D} \Delta \boldsymbol{\varepsilon} d\Omega + \beta \int_{\Gamma_u} \delta \mathbf{u}^T \Delta \mathbf{u} d\Gamma + \int_{\Omega} \delta \boldsymbol{\varepsilon}^t \boldsymbol{\sigma} d\Omega - \int_{\Omega} \delta \mathbf{u}^t \mathbf{b} d\Omega \\ - \int_{\Gamma_t} \delta \mathbf{u}^t \bar{\mathbf{t}} d\Gamma + \beta \int_{\Gamma_u} \delta \mathbf{u}^t (\mathbf{u} - \bar{\mathbf{u}}) d\Gamma = 0. \end{aligned} \quad (27)$$

where \mathbf{D} is the consistent tangent modulus which will be described in section 4.3.

3.2 Discretization

According to the approximation obtained from RKPM approximation mentioned in Eq. (15), the discretized global form of a 2D displacement field is

$$\mathbf{u} \cong \mathbf{u}^R = \mathbf{\Psi}\hat{\mathbf{u}}, \quad (28)$$

where $\mathbf{\Psi}$ is the matrix of the shape functions that is defined

$$\mathbf{\Psi} = \begin{bmatrix} \psi^1 & 0 & \psi^2 & 0 & \dots & \psi^{NP} & 0 \\ 0 & \psi^1 & 0 & \psi^2 & \dots & 0 & \psi^{NP} \end{bmatrix}, \quad (29)$$

and the vector of nodal degrees of freedom (DOFs) $\hat{\mathbf{u}}$ is

$$\hat{\mathbf{u}}^t = [\hat{u}_1^1 \quad \hat{u}_2^1 \quad \hat{u}_1^2 \quad \hat{u}_2^2 \quad \dots \quad \hat{u}_1^{NP} \quad \hat{u}_2^{NP}], \quad (30)$$

in which \hat{u}_j^l represents the fictitious nodal value of the l th particle along x_j direction. By the assumption of small strain, the strain components are defined

$$\varepsilon_{ij} = (u_{i,j} + u_{j,i})/2, \quad u_{i,j} = \partial u_i / \partial x_j, \quad i, j = 1, 2. \quad (31)$$

The variational (via Galerkin method) and incremental displacements and strains are

$$\delta \mathbf{u} = \mathbf{\Psi} \delta \hat{\mathbf{u}}, \quad (\text{a}) \quad \mathbf{u} = \mathbf{\Psi} \Delta \hat{\mathbf{u}}, \quad (\text{b})$$

$$\delta \boldsymbol{\varepsilon} = \mathbf{B} \delta \hat{\mathbf{u}}, \quad (\text{c}) \quad \Delta \boldsymbol{\varepsilon} = \mathbf{B} \phi \hat{\mathbf{u}}, \quad (\text{d}) \quad (32)$$

where $\Delta \hat{\mathbf{u}}$ is the increment of $\hat{\mathbf{u}}$ vector, and \mathbf{B} is the matrix of the gradients of the shape functions with respect to x_1 and x_2

$$\mathbf{B} = \begin{bmatrix} \frac{\phi \psi^1}{\partial x_1} & 0 & \frac{\phi \psi^2}{\partial x_1} & 0 & \dots & \frac{\phi \psi^{NP}}{\partial x_1} & 0 \\ 0 & \frac{\phi \psi^1}{\partial x_2} & 0 & \frac{\phi \psi^2}{\partial x_2} & \dots & 0 & \frac{\phi \psi^{NP}}{\partial x_2} \\ \frac{\phi \psi^1}{\partial x_2} & \frac{\phi \psi^1}{\partial x_1} & \frac{\phi \psi^2}{\partial x_2} & \frac{\phi \psi^2}{\partial x_1} & \dots & \frac{\phi \psi^{NP}}{\partial x_2} & \frac{\phi \psi^{NP}}{\partial x_1} \end{bmatrix}. \quad (33)$$

Substituting Eqs. (32) into Eq. (27) and considering a load-control case lead to the following matrix form equation

$$(\mathbf{K} + \mathbf{K}^u) \Delta \hat{\mathbf{u}}_{n+1}^{k+1} = \mathbf{f}_{n+1}^{\text{ext}} - \mathbf{f}^{\text{int}}(\hat{\mathbf{u}}_{n+1}^k) = -\mathbf{r}^k, \quad (34)$$

in which $n + 1$ and $k + 1$ represent the current step and iteration respectively, and

$$\mathbf{K} = \int_{\Omega} \mathbf{B}^t \mathbf{D} \mathbf{B} d\Omega,$$

$$\begin{aligned}
\mathbf{K}^u &= \beta \int_{\Gamma_u} \boldsymbol{\Psi}^t \mathbf{S}^u \boldsymbol{\Psi} d\Gamma, \\
\widehat{\mathbf{u}}_{n+1}^{k+1} &= \widehat{\mathbf{u}}_{n+1}^k + \Delta \widehat{\mathbf{u}}_{n+1}^{k+1}, \\
\mathbf{f}_{n+1}^{\text{ext}} &= \int_{\Omega} \boldsymbol{\Psi}^t \mathbf{b}_{n+1} d\Omega + \int_{\Gamma_t} \boldsymbol{\Psi}^t \bar{\mathbf{t}}_{n+1} d\Gamma + \beta \int_{\Gamma_u} \boldsymbol{\Psi}^t \bar{\mathbf{u}} d\Gamma, \\
\mathbf{f}_{n+1}^{\text{int}}(\widehat{\mathbf{u}}_{n+1}^k) &= \int_{\Omega} \mathbf{B}^t \boldsymbol{\sigma}(\widehat{\mathbf{u}}_{n+1}^k) d\Omega + \mathbf{K}^u \widehat{\mathbf{u}}_{n+1}^k, \tag{35}
\end{aligned}$$

where \mathbf{r}_{n+1}^{k+1} is the residual vector associated with the current iteration and step. Matrix \mathbf{S}^u is defined

$$\mathbf{S}^u = \begin{bmatrix} S_1 & 0 \\ 0 & S_2 \end{bmatrix}, \quad S_i = \begin{cases} 1 & \text{if } u_i \text{ is prescribed on } \Gamma_u, \\ 0 & \text{if } u_i \text{ is not prescribed on } \Gamma_u. \end{cases} \tag{36}$$

The relative and absolute convergence criteria of Eq. (34) respectively are [De Souza Neto, Peric, and Owen (2008)]

$$\frac{\mathbf{r}_{n+1}^{k+1}}{\mathbf{f}_{n+1}^{\text{ext}}} \leq \phi_{\text{tol}}^1, \quad \mathbf{r}_{n+1}^{k+1} \infty \leq \phi_{\text{tol}}^2, \tag{37}$$

where ϕ_{tol}^1 and ϕ_{tol}^2 are sufficiently small specified equilibrium convergence tolerances.

4 Implementation of material nonlinearity

In the present article, the fully implicit integration algorithm, namely backward Euler method, is adopted so as to solve constitutive elastic-plastic differential equations. The specialization considered assumes von Mises model, associated flow rule, linear elastic behavior and general nonlinear isotropic strain hardening [De Souza Neto, Peric, and Owen (2008)].

4.1 Fundamental equations to implement von Mises model

The model is composed of:

a. The linear elastic law

$$\boldsymbol{\sigma} = \mathbf{D}^e \boldsymbol{\varepsilon}^e, \tag{38}$$

where $\boldsymbol{\varepsilon}^e$ is the elastic strain vector, and \mathbf{D}^e is the matrix of isotropic elastic material properties that is in plane strain case

$$\mathbf{D}^e = \frac{E}{(1+\nu)(1-2\nu)} \begin{bmatrix} 1-\nu & \nu & 0 \\ \nu & 1-\nu & 0 \\ 0 & 0 & 0.5-\nu \end{bmatrix}. \tag{39}$$

E and ν are Young's modulus and Poisson's ratio, respectively.

b. The von Mises yield function

$$\Phi(\boldsymbol{\sigma}, \sigma_y) = \sqrt{3J_2(\boldsymbol{\sigma})} - \sigma_y(\bar{\epsilon}_p) = \sigma^{\text{eff}} - \sigma_y(\bar{\epsilon}_p), \quad (40)$$

in which $\bar{\epsilon}_p$ is the accumulated effective plastic strain, σ^{eff} is the effective stress, and the second invariant of deviatoric stresses are defined

$$J_2(\boldsymbol{\sigma}) = \frac{1}{2}s_{ij}s_{ij}, \quad i, j = 1, 2, 3, \quad (41)$$

and \mathbf{S} is the tensor of deviatoric stresses whose components are defined

$$\mathbf{S} = \boldsymbol{\sigma} - p\mathbf{I}, \quad p = \frac{\sigma_{ii}}{3}, \quad i = 1, 2, 3 \quad \text{Hydrostatic stress}, \quad (42)$$

where \mathbf{I}_3 is the identity matrix.

c. The associated Prandtl-Reuss flow rule

$$\dot{\boldsymbol{\epsilon}}^p = \frac{\partial \phi}{\partial \boldsymbol{\sigma}} \dot{\lambda} = \frac{3}{2} \frac{\mathbf{S}}{\sigma^{\text{eff}}} \dot{\lambda}, \quad (43)$$

where dot represents the rate of a specific parameter, and $\dot{\lambda}$ is the plastic multiplier. The effective plastic strain rate in terms of plastic strain rate norm is

$$\dot{\bar{\epsilon}}^p = \sqrt{\frac{2}{3} \dot{\epsilon}_{ij}^p \dot{\epsilon}_{ij}^p} = \dot{\lambda}. \quad (44)$$

4.2 The implicit elastic predictor/plastic corrector procedure

Due to accumulated $\Delta \hat{\mathbf{u}}$ in current step, $(n+1)$, $\Delta \boldsymbol{\epsilon}$ is calculated by Eq. (32d) denoting

$$\Delta \boldsymbol{\epsilon} = \boldsymbol{\epsilon}_{n+1} - \boldsymbol{\epsilon}_n. \quad (45)$$

At the beginning, $\Delta \boldsymbol{\epsilon}$ is accounted purely elastic. So,

$$\boldsymbol{\epsilon}_{n+1}^{\text{e trial}} = \boldsymbol{\epsilon}_n^{\text{e}} + \Delta \boldsymbol{\epsilon}, \quad \bar{\epsilon}_{n+1}^{\text{p trial}} = \bar{\epsilon}_n^{\text{p}}, \quad (46)$$

accordingly, corresponding trial deviatoric and hydrostatic stresses are

$$\mathbf{S}_{n+1}^{\text{trial}} = 2G\boldsymbol{\epsilon}_{n+1}^{\text{e trial}}, \quad p_{n+1}^{\text{trial}} = K\epsilon_{n+1}^{\text{e trial}}, \quad (47)$$

where volumetric and deviatoric strains respectively are

$$\boldsymbol{\varepsilon}_d = \boldsymbol{\varepsilon} - \varepsilon_v \mathbf{I}, \quad \varepsilon_v = \frac{\varepsilon_{ii}}{3}, \quad i = 1, 2, 3; \quad (48)$$

also, G and K are shear and bulk moduli, respectively. The trial yield stress in current step is

$$\boldsymbol{\sigma}_{y\ n+1}^{\text{trial}} = \boldsymbol{\sigma}_{y\ n}, \quad (49)$$

where

$$\boldsymbol{\sigma}_{y\ n} = \boldsymbol{\sigma}_y (\bar{\boldsymbol{\varepsilon}}_n^p). \quad (50)$$

Now, the admissibility of trial stress state should be checked

$$\Phi(\boldsymbol{\sigma}_{n+1}^{\text{trial}}, \boldsymbol{\sigma}_{y\ n}) \leq 0. \quad (51)$$

If inequity (51) is true, the state is fully elastic. Therefore,

$$\boldsymbol{\varepsilon}_{n+1}^e = \boldsymbol{\varepsilon}_{n+1}^{\text{trial}}, \quad \boldsymbol{\sigma}_{n+1} = \mathbf{S}_{n+1}^{\text{trial}} + p_{n+1}^{\text{trial}} \mathbf{I}, \quad \bar{\boldsymbol{\varepsilon}}_{n+1}^p = \bar{\boldsymbol{\varepsilon}}_{n+1}^{\text{trial}} \quad (52)$$

are updated. Otherwise, the present state is elastic-plastic, and the return-mapping procedure has to be applied. With the notion of von Mises model, the return-mapping process leads to solving the following system of nonlinear equations

$$\begin{aligned} \boldsymbol{\varepsilon}_{n+1}^e &= \boldsymbol{\varepsilon}_{n+1}^{\text{trial}} - \Delta\lambda \frac{3}{2} \frac{\mathbf{S}_{n+1}}{\boldsymbol{\sigma}^{\text{eff}}(\mathbf{S}_{n+1})}, \\ \bar{\boldsymbol{\varepsilon}}_{n+1}^p &= \bar{\boldsymbol{\varepsilon}}_n^p + \Delta\lambda, \\ \boldsymbol{\sigma}^{\text{eff}}(\mathbf{S}_{n+1}) - \boldsymbol{\sigma}_y(\bar{\boldsymbol{\varepsilon}}_{n+1}^p) &= 0 \end{aligned} \quad (53)$$

for $\boldsymbol{\varepsilon}_{n+1}^e$, $\bar{\boldsymbol{\varepsilon}}_{n+1}^p$, and $\Delta\lambda$ (the incremental plastic multiplier). It can be shown that for von Mises model

$$\mathbf{S}_{n+1} = \left(1 - \frac{3G\Delta\lambda}{\boldsymbol{\sigma}^{\text{eff}}(\mathbf{S}_{n+1}^{\text{trial}})} \right) \mathbf{S}_{n+1}^{\text{trial}}. \quad (54)$$

Substituting Eq. (54) and (53)_b into (53)_c, and after some simplifications, boils down to the following single-variable (generally nonlinear) equation

$$\boldsymbol{\sigma}^{\text{eff}}(\mathbf{S}_{n+1}^{\text{trial}}) - 3G\Delta\lambda - \boldsymbol{\sigma}_y(\bar{\boldsymbol{\varepsilon}}_n^p + \Delta\lambda) = 0, \quad (55)$$

which is solved for $\Delta\lambda$ by using the Newton-Raphson method [De Souza Neto, Peric, and Owen (2008)]. Subsequently, the current state variables are updated as follows

$$\begin{aligned}
 \mathbf{S}_{n+1} &= \left(1 - \frac{3G\Delta\lambda}{\sigma^{\text{eff}}(\mathbf{S}_{n+1}^{\text{trial}})} \right) \mathbf{S}_{n+1}^{\text{trial}}, \\
 \boldsymbol{\sigma}_{n+1} &= \mathbf{S}_{n+1} + p_{n+1}^{\text{trial}} \mathbf{I}, \\
 \boldsymbol{\varepsilon}_{n+1}^e &= \frac{1}{2G} \mathbf{S}_{n+1} + \frac{1}{3} \boldsymbol{\varepsilon}_{v n+1}^e, \\
 \bar{\boldsymbol{\varepsilon}}_{n+1}^p &= \bar{\boldsymbol{\varepsilon}}_n^p + \Delta\lambda, \\
 \boldsymbol{\varepsilon}_{n+1}^p &= \boldsymbol{\varepsilon}_n^p + \Delta\lambda \frac{3}{2} \frac{\mathbf{S}_{n+1}}{\sigma^{\text{eff}}(\mathbf{S}_{n+1})}.
 \end{aligned} \tag{56}$$

4.3 Consistent tangent modulus [De Souza Neto, Peric, and Owen (2008)]

If Eq. (51) holds, then the consistent tangent modulus, \mathbf{D} , is the same as \mathbf{D}^e in Eq. (39); otherwise, for the von Mises model with isotropic strain hardening \mathbf{D} is calculated as

$$\mathbf{D} = \mathbf{D}^{\text{ep}} = \mathbf{D}_c^{\text{ep}} - \frac{6G^2\Delta\lambda}{\sigma^{\text{eff}}(\mathbf{S}_{n+1}^{\text{trial}})} (\mathbf{I}_d - \bar{\mathbf{N}}^T \bar{\mathbf{N}}), \tag{57}$$

where

$$\mathbf{I}_d = \begin{bmatrix} \frac{2}{3} & -\frac{1}{3} & 0 \\ -\frac{1}{3} & \frac{2}{3} & 0 \\ 0 & 0 & \frac{1}{2} \end{bmatrix}, \tag{58}$$

$\bar{\mathbf{N}}$ in vector form is

$$\bar{\mathbf{N}} = \sqrt{\frac{3}{2}} \frac{\mathbf{S}_{n+1}^{\text{trial}}}{\sigma^{\text{eff}}(\mathbf{S}_{n+1}^{\text{trial}})}, \tag{59}$$

and \mathbf{D}_c^{ep} is continuum elastic-plastic tangent modulus which is

$$\mathbf{D}_c^{\text{ep}} = \mathbf{D}^e - \frac{6G^2}{3G+H} \bar{\mathbf{N}}^T \bar{\mathbf{N}}, \tag{60}$$

where H is the slope of strain-hardening curve

$$H = \left. \frac{d\sigma_y}{d\bar{\boldsymbol{\varepsilon}}^p} \right|_{\bar{\boldsymbol{\varepsilon}}_n^p + \Delta\lambda}. \tag{61}$$

The difference between the consistent tangent modulus, \mathbf{D}^{ep} , and its continuum counterpart, \mathbf{D}_c^{ep} , arises from adopting the backward Euler scheme, hence, using \mathbf{D}_c^{ep} [Own and Hinton (1980)] is not appropriate for global Newton-Raphson procedure in Eq. (27).

4.4 One-dimensional stress-strain relationship and strain hardening curve

A modified form of the Ramberg-Osgood relationship is used in place of the original one; because, the behavior of the material in the elastic region is supposed to be linear. The σ vs. ε curve assuming the modified Ramberg-Osgood law is described by

$$\frac{\varepsilon}{\varepsilon_0} = \begin{cases} \frac{\sigma}{\sigma_0}, & \sigma \leq \sigma_0, \\ \left(\frac{\sigma}{\sigma_0}\right)^n, & \sigma > \sigma_0. \end{cases} \quad (62)$$

σ_0 and ε_0 are the primary yield stress and primary yield strain respectively which are related to each other by $\sigma_0 = E\varepsilon_0$. Also, n is the hardening power. $\sigma - \varepsilon$ diagrams, complying modified Ramberg-Osgood relationship, for high, medium, and low hardening materials in which n is equal to 3, 10, and 50 respectively, are plotted in Fig. 1, as well as for an elastic-perfectly plastic material behavior. Uniaxial strains are limited to 10% (the maximum acceptable strain for small deformation formulation [Anderson (1995)]).

According to Eq. (62), the strain-hardening curve is

$$\frac{\bar{\varepsilon}^p}{\varepsilon_0} = \left(\frac{\sigma_y}{\sigma_0}\right)^n - \frac{\sigma_y}{\sigma_0} \quad \text{if} \quad \sigma^{\text{eff}} > \sigma_0, \quad (63)$$

where $\bar{\varepsilon}^p$ and σ_y are effective plastic strain and current yield stress respectively. Each generally nonlinear curve can be almost accurately replaced with a piecewise linear function by means of sufficient number of points; thereupon, in order to have more conformity with experimental data, the strain-hardening continuous graph is substituted by a set of points derived from Eq. (63). After the last point in the hardening curve, it is supposed that no hardening will occur.

5 Crack modeling in meshfree methods

The crack is modeled by a line segment as an internal boundary. On the account of discontinuous displacement field across the crack faces, some modifications on particle arrangement and the approximation of RKPM should be employed, which will be discussed in the following.

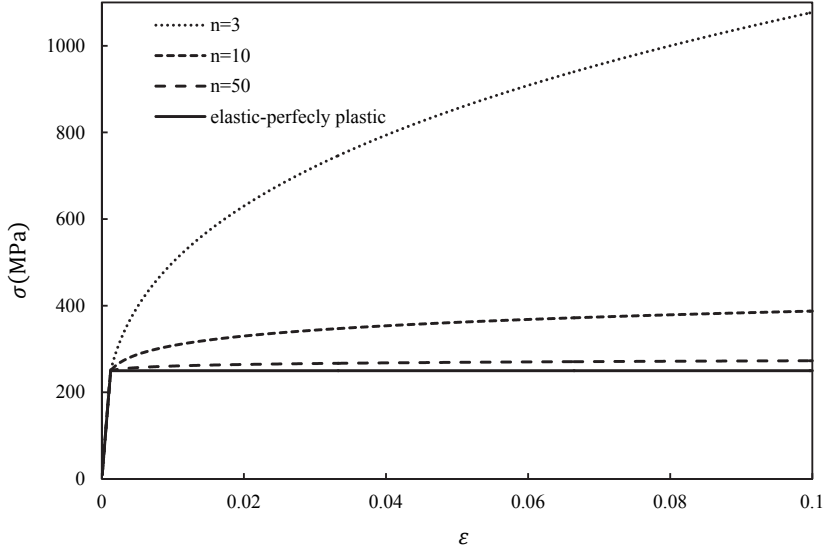


Figure 1: High, medium, low, and no hardening stress vs. strain diagrams

5.1 Distribution of particles

First, a uniform distribution of particles over the entire domain is considered. Then, the particles located on the crack line are split in two and slightly shifted to opposite sides of the crack by equal distance in the order of about 10^{-4} . Since linear basis is utilized, a sufficiently dense pattern of particles should be added to the crack tip region in order to capture the high-gradient fields more accurately. To this end, three conventional patterns of particles in Fig. 3 are considered. If the radii of the rings of particles are set to increase monotonically, a large number of particles should be located around the crack tip. To date, no efficient systematic method to determine the location of the particles in the refinement zone has been proposed. In this paper, we introduce an efficient procedure in which a definite number of particles are distributed in a progressive manner. This leads to a remarkable improvement of solutions.

Assume a_0 is the radius of the first ring surrounding the crack tip. Then, R_i , the radius of the i th ring becomes

$$R_i = \frac{i}{2} [2a_0 + (i-1)d], \quad (64)$$

where the constant, d , is the difference between two successive members of the

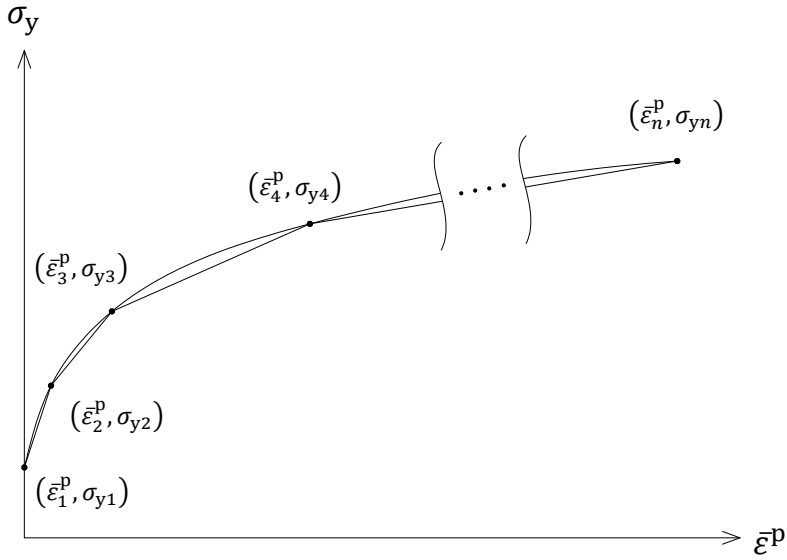


Figure 2: Piecewise linear strain hardening diagram.

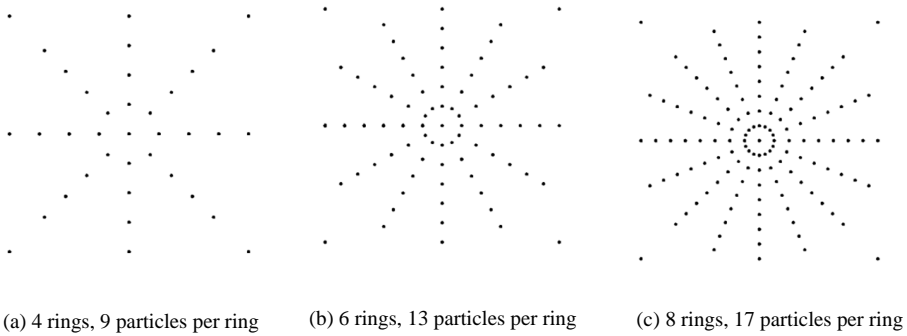


Figure 3: Monotonous refinements: (a) array 1 (b) array 2 (c) array 3

arithmetic progression. Hence,

$$d = \frac{2}{n-1} \left(\frac{\Delta x^{\text{uniform}}}{n} - a_0 \right), \tag{65}$$

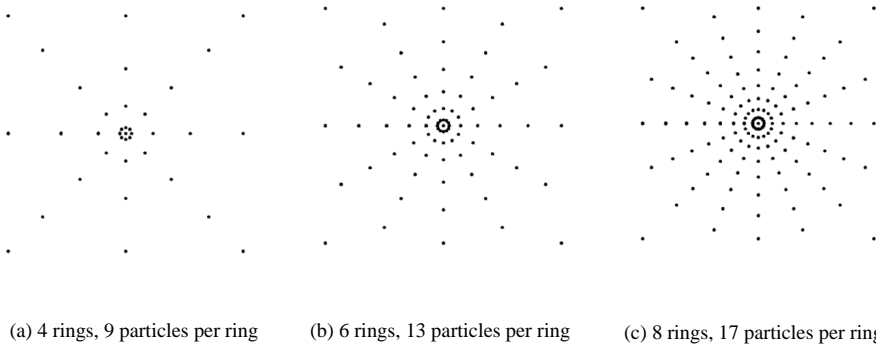


Figure 4: Progressive refinements: (a) array 1 (b) array 2 (c) array 3

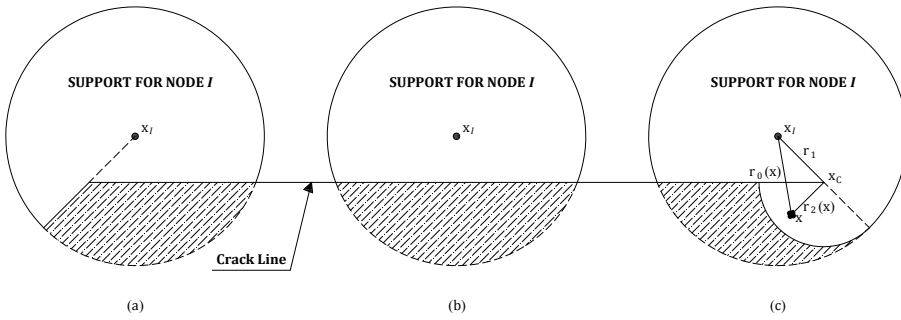


Figure 5: Visibility and diffraction criteria: (a) visibility modification (b) visibility or diffraction modification (c) diffraction modification

where n is the total number of rings, and $\Delta x^{\text{uniform}}$ is the distance between two horizontally or vertically adjacent particles in the uniform distribution. In present work, a_0 is set $0.05\Delta x^{\text{uniform}}$. The progressive refinement arrays are shown in Fig. 4.

5.2 Treatments to domain discontinuity

Through engineering problems, the domain of the problem may contain non-convex boundaries, particularly the fracture ones having discontinuous displacement fields. In such conditions, the window functions associated with particles, whose support-

sare sliced by the discontinuity, should be modified. In the literature, various criteria have been suggested such as visibility and diffraction, in which the window function is revised.

5.2.1 Visibility criterion

One of the discontinuity criteria is the visibility introduced by [Belytschko, Lu, Gu (1994); Krysl and Belytschko (1996)]. In this approach, boundaries of the body and any interior lines of discontinuity are considered as opaque obstacles. The line segment constructed between a particle and a calculation point is regarded as a ray of light. Provided that, this ray intersects the line of discontinuity, the point is removed from the domain of influence of the particle (see Fig. 5a and 5b). Henceforth, the modified shape functions are attained on the basis of current revised window functions. Employing this criterion results in discontinuous window functions which generate discontinuous shape functions around the crack tip that are not desirable for Galerkin method.

5.2.2 Diffraction method

The smooth shape functions can be obtained by modifying window functions smoothly. In the diffraction (wrap-around) method [Organ, Fleming, Terry, and Belytschko (1996); Belytschko, Krongauz, Organ, Fleming, and Krysl (1996)], when the ray of light (described in 4.2.1) intersects the line of discontinuity (see Fig. 5), the distance between the particle and the calculation point is revised by

$$d_I(\mathbf{x}) = \left(\frac{r_1 + r_2(\mathbf{x})}{r_0(\mathbf{x})} \right)^\zeta r_0(\mathbf{x}), \quad (66)$$

where

$$r_0(\mathbf{x}) = \mathbf{x} - \mathbf{x}_I, \quad r_1 = \mathbf{x}_c - \mathbf{x}_I, \quad r_2(\mathbf{x}) = \mathbf{x} - \mathbf{x}_c, \quad (67)$$

in which regarding Fig. 5, $r_0(\mathbf{x})$ is the distance between the calculation point and the particle, r_1 is the distance between the crack tip and the particle, and $r_2(\mathbf{x})$ is the distance from the calculation point to the crack tip. The derivatives of the window function ϕ considering the chain rule are

$$\frac{d\phi}{dx_i} = \frac{\partial\phi}{\partial d_I} \frac{\partial d_I}{\partial x_i}. \quad (68)$$

$\partial\phi/\partial d_I$ is derived from the Eq. (18). Therefore, all that is required is to determine $\partial d_I/\partial x_i$ explicitly

$$\frac{\partial d_I}{\partial x_i} = \zeta \left(\frac{r_1 + r_2(\mathbf{x})}{r_0(\mathbf{x})} \right)^{\zeta-1} \frac{\partial r_2(\mathbf{x})}{\partial x_i} + (1 - \zeta) \left(\frac{r_1 + r_2(\mathbf{x})}{r_0(\mathbf{x})} \right)^\zeta \frac{\partial r_0(\mathbf{x})}{\partial x_i}, \quad (69)$$

where

$$\frac{\partial r_0(\mathbf{x})}{\partial x_i} = \frac{x_i - x_{li}}{r_0}, \quad \frac{\partial r_2(\mathbf{x})}{\partial x_i} = \frac{x_i - x_{ci}}{r_2}. \quad (70)$$

In the literature, assuming the values 1 and 2 for diffraction parameter, ζ , are recommended [Organ, Fleming, Terry, and Belytschko (1996) and Belytschko (1997)]; however, no tracking has been performed to determine the best value for ζ in EPFM. In the section of “Results and discussions” we will deal with this issue.

6 J integral

One of the parameters which is widely used in fracture mechanics and characterizes the crack tip singularity is the J integral. General definition of the J parameter when the crack tip is surrounded by a vanishingly small contour under quasi-static loading is [Cherepanov (1967) and Eshelby (1970)]

$$J = \lim_{\Gamma_0 \rightarrow 0} \int_{\Gamma_0} \left[w \delta_{li} - \sigma_{ij} \frac{\partial u_j}{\partial x_1} \right] n_i d\Gamma, \quad (71)$$

in which $w = \int_0^{\epsilon_{kl}^{\text{total}}} \sigma_{ij} d\epsilon_{ij}$ is the strain energy density that can be defined for general material behavior, and \mathbf{n} is the unit outward vector normal to Γ_0 . Considering an elastic-plastic material behavior, the total strain is given by

$$\epsilon_{ij}^{\text{total}} = \epsilon_{ij}^e + \epsilon_{ij}^p. \quad (72)$$

Consequently, w can be divided into elastic and plastic components as

$$w = w^e + w^p = \int_0^{\epsilon_{kl}^e} \sigma_{ij} d\epsilon_{ij}^e + \int_0^{\epsilon_{kl}^p} \sigma_{ij} d\epsilon_{ij}^p. \quad (73)$$

For the reason that evaluating the stress and strain fields along a vanishingly small contour is not practicable in numerical analysis, other forms of Eq. (71) should be taken into account. One of these forms is the contour integral [Rice (1968), Budiansky and Rice (1973), and Bakker (1984)] which in 2D case is Rice’s J integral

$$J = \int_{\Gamma^*} \left[w \delta_{li} - \sigma_{ij} \frac{\partial u_j}{\partial x_1} \right] n_i d\Gamma, \quad (74)$$

in which Γ^* is any arbitrary contour surrounding the crack tip as shown in Fig. 6. Another form of Eq. (71), introduced by [Li, Shih, and Needleman (1985), Shih, Moran, and Nakamura (1986), Nikishkov and Atluri (1987a, b), Nikishkov and

Atluri (1987), and Moran and Shih (1987)], is domain integral which in the absence of thermal strains, body forces, and crack face tractions in 2D specialization is

$$J = \int_{A^*} \left\{ \left[\sigma_{ij} \frac{\partial u_j}{\partial x_1} - w \delta_{1i} \right] \frac{\partial q}{\partial x_i} + \left[\sigma_{ij} \frac{\partial \varepsilon_{ij}^p}{\partial x_1} - \frac{\partial w^p}{\partial x_1} \right] q \right\} dA, \quad (75)$$

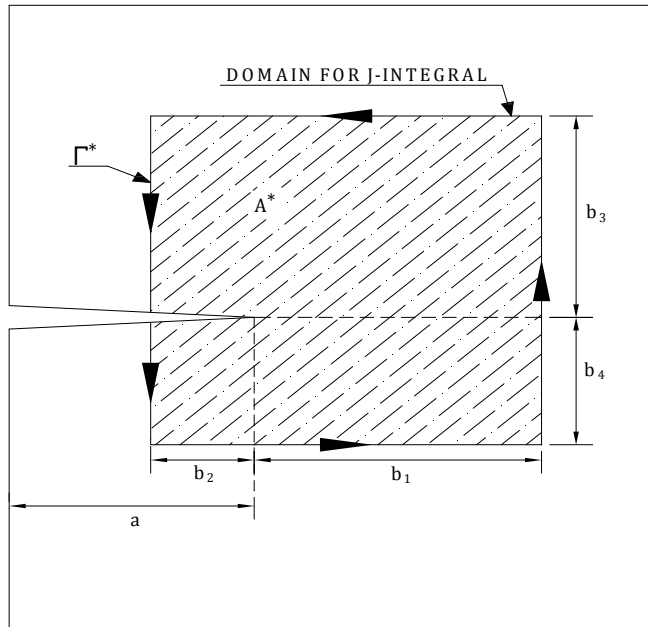


Figure 6: Domain and contour used in J integral

where A^* is an enclosed area by Γ^* as shown in Fig. 6, and q is an arbitrary but smooth function having the unit value on the crack tip and zero on Γ^* . In this research, q complies the following equation

$$q = \begin{cases} \left(1 - \frac{x-x_c}{b_1}\right) \left(1 - \frac{y-y_c}{b_3}\right) & x > x_c \text{ and } y \geq y_c \\ \left(1 + \frac{x-x_c}{b_2}\right) \left(1 - \frac{y-y_c}{b_3}\right) & x \leq x_c \text{ and } y > y_c \\ \left(1 + \frac{x-x_c}{b_2}\right) \left(1 + \frac{y-y_c}{b_4}\right) & x < x_c \text{ and } y \leq y_c \\ \left(1 - \frac{x-x_c}{b_1}\right) \left(1 + \frac{y-y_c}{b_4}\right) & x \geq x_c \text{ and } y < y_c \end{cases} \quad (76)$$

In the above equation, x_c and y_c are the crack tip coordinates.

Due to difficulties encountered in deriving the closed forms for the terms $\partial \varepsilon_{ij}^p / \partial x_1$ and $\partial w^p / \partial x_1$, we employed the reproducing approximations like (15)

$$\begin{aligned} \frac{\partial \varepsilon_{ij}^p}{\partial x_1}(\mathbf{x}) &= \int_{I=1}^{NP} \Psi_{,x_1}^I(\mathbf{x}) \varepsilon_{ij}^{pI}, \\ \frac{\partial w^p}{\partial x_1}(\mathbf{x}) &= \int_{I=1}^{NP} \Psi_{,x_1}^I(\mathbf{x}) w^{pI}, \end{aligned} \quad (77)$$

where ε_{ij}^{pI} and w^{pI} are the nodal values of ε_{ij}^p and w^p , respectively.

7 Numerical results

To exhibit the efficacy of RKPM in analyzing EPFM problems, some numerical examples are examined. Two characteristics parameters, J integral and CMOD, together with the distribution of stress fields are investigated for plane strain condition. Far-field loadings are employed in such a way that contained yielding condition [Simha, Fischer, Shan, and Kolednik (2008)] holds. To verify these evaluated parameters, comparisons are made with the FEM results obtained from ABAQUS.

In FEM modeling, quadratic plane strain elements are used throughout the entire domain. To model singularity at the crack tip, for hardening behavior, eight node collapsed elements whose mid-side nodes are shifted one fourth of element dimension to the crack tip are employed and three collapsed nodes at the crack tip of each element are free to move independently. For non-hardening material the same elements are used; but, mid-side nodes are not shifted. Fifty different paths surrounding the crack tip are considered and the value of J integral over the last path is reported as the real far-field or saturated one [Yuan and Brocks (1991) and Simha, Fischer, Shan, Chen, and Kolednik (2008)]. Through RKPM modeling, to evaluate domain and contour J integrals twenty sets of dimensions (see Tab. 1) are adopted.

7.1 Effect of progression on refinement

Considering Fig. 7, the dimensions used in this test are: width $W = 1m$, length $L = 4m$, and crack length $a = 0.2m$. These values are adopted in such a way that the effect of length, L , on solution is eliminated [Shih and Needleman (1984)]. The material parameters involved in elastic-plastic behavior are: $E = 200\text{GPa}$, $\nu = 0.3$, $\sigma_0 = 250\text{MPa}$, and hardening parameter $n = 10$. The far-field tensile stress $\sigma^\infty = 125\text{MPa}$. Penalty coefficient, β , is adopted $10^6 E$, in which E is Young's modulus [Zhu and Atluri (1998)]. 1705 particles are distributed regularly throughout the domain (Fig. 8); in addition, six different arrays of refinement (Figs. 3 and 4)

Table 1: Sets of dimensions used in calculating J integral

Set counter	$b_1 (m)$	$b_2 (m)$	$b_3 (m)$	$b_4 (m)$	$A^* (m^2)$
1	0.1	0.1	0.1	0.1	0.04
2	0.2	0.2	0.2	0.2	0.16
3	0.2	0.3	0.3	0.3	0.3
4	0.2	0.4	0.4	0.4	0.48
5	0.2	0.5	0.5	0.5	0.7
6	0.2	0.6	0.6	0.6	0.96
7	0.2	0.7	0.7	0.7	1.26
8	0.2	0.8	0.8	0.8	1.6
9	0.2	0.8	0.9	0.9	1.8
10	0.2	0.8	1	1	2
11	0.2	0.8	1.1	1.1	2.2
12	0.2	0.8	1.2	1.2	2.4
13	0.2	0.8	1.3	1.3	2.6
14	0.2	0.8	1.4	1.4	2.8
15	0.2	0.8	1.5	1.5	3
16	0.2	0.8	1.6	1.6	3.2
17	0.2	0.8	1.7	1.7	3.4
18	0.2	0.8	1.8	1.8	3.6
19	0.2	0.8	1.9	1.9	3.8
20	0.2	0.8	2	2	4

are adopted in the vicinity of the crack tip. For numerical purposes, background integration cells are created like FEM mesh; 4×4 Gauss quadrature is used in each cell. FEM meshing is illustrated in Fig. 9 with 1088 elements and 3433 nodes.

First of all, considering Figs. 3 and 4 the effect of employing progression in the arrangement of particles throughout the refinement zone on the J integral values in domain form, where diffraction method with $\zeta = 2$ is adopted, is shown in Fig. 10. The reference J integral is $J^{FEM} = 0.0898 \text{ KJ/m}^2$. It is evident that J integral values for each array are improved by about 1 to 2 percents. It can be observed, as the ratio A^*/A^{Plate} increases, the values of J integral monotonously tend to constant saturated ones for paths far enough from the crack tip region. To assure how the approximation in Eq. (77) works, the J integral values in contour form are depicted in Fig. 11. The same behavior stated above for domain form holds; especially, in the case of dense arrays, the results have a good agreement with FEM.

The other characteristic parameter in EPFM, CMODs, for progressive and monotonous

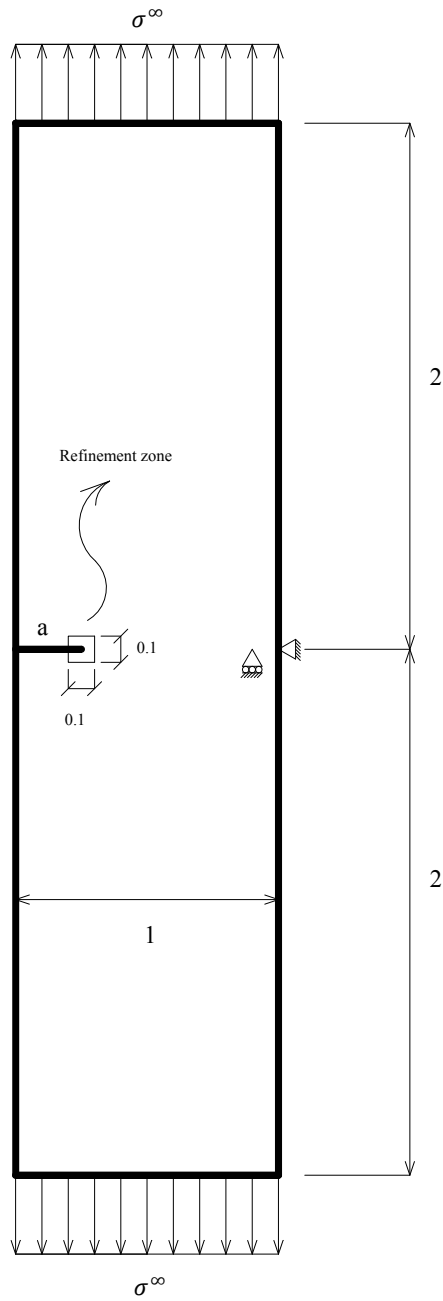


Figure 7: Edge-cracked plate under far-field tensile stress

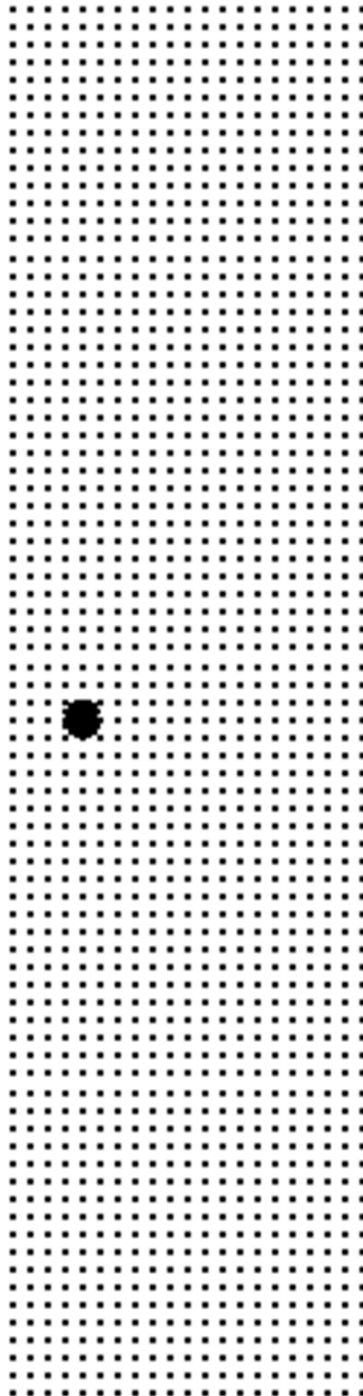


Figure 8: Meshless discretization of the edge-cracked plate

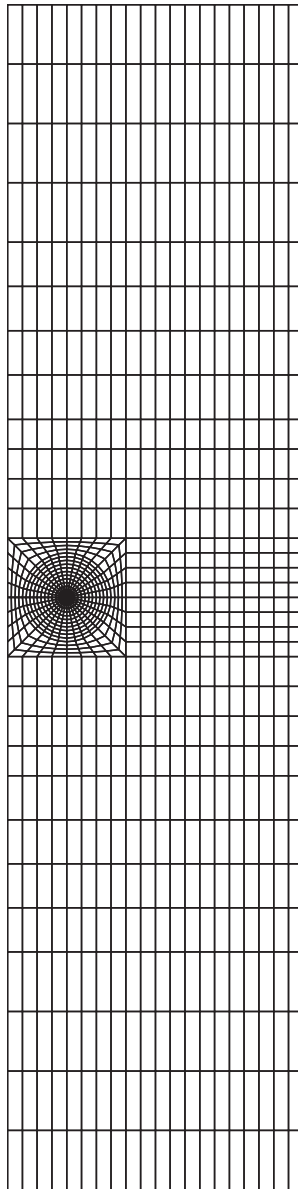


Figure 9: FEM meshing of the edge-cracked plate

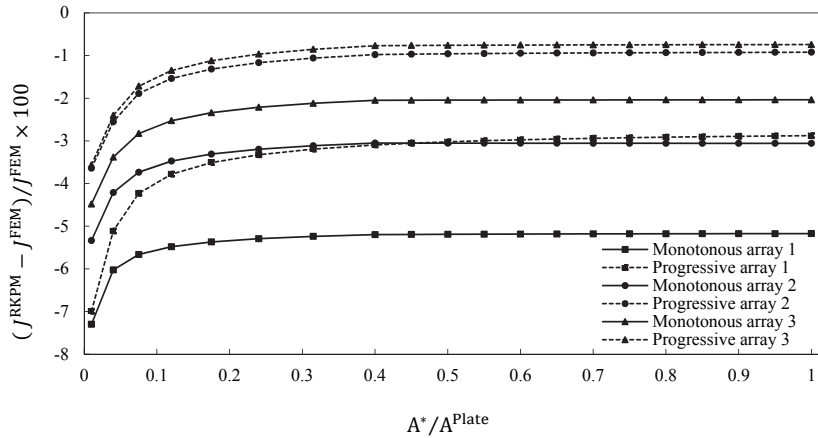


Figure 10: Domain J integral difference ratio vs. relative domain area for monotonous and progressive arrays of particles around crack tip

arrays of particles are shown and compared with FEM one in Tab. 2. As expected, progressive arrays 2 and 3 yield CMODs having under 1% difference with FEM counterparts.

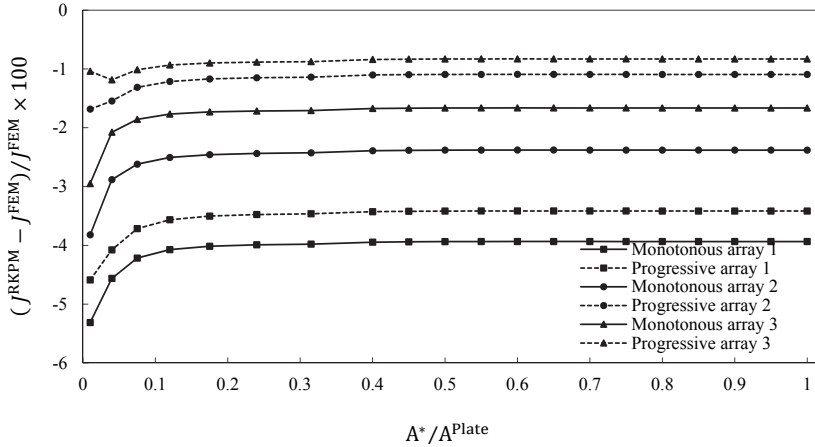
Table 2: CMOD for monotonous and progressive arrays of particles around the crack tip

	RKPM	$(\text{CMOD}^{\text{FEM}} - \text{CMOD}^{\text{RKPM}}) / \text{CMOD}^{\text{FEM}} \times 100$
Monotonous array 1	0.000837363	4.17
Progressive Array 1	0.000858164	1.79
Monotonous array 2	0.000849778	2.75
Progressive Array 2	0.00086642	0.84
Monotonous array 3	0.000860717	1.50
Progressive Array 3	0.000868835	0.57

To demonstrate how effective stresses are distributed around the crack tip, the contours of plastic zone resulting from different arrays of particles are sketched in Fig. 12. It can be concluded that even in dense patterns of particles without considering progression, the desirable shapes of plastic zone are not obtained.

Table 3: CMOD for visibility and diffraction methods

	RKPM	$(\text{CMOD}^{\text{FEM}} - \text{CMOD}^{\text{RKPM}}) / \text{CMOD}^{\text{FEM}} \times 100$
Visibility method	0.001003746	-14.87
Diffraction method	0.000868835	0.57


 Figure 11: Contour J integral difference ratios. relative domain area for monotonous and progressive arrays of particles around crack tip

7.2 Comparison between discontinuity treatments

Considering the appropriate refinement, which is progressive array 3, now we are interested in how different discontinuity criteria can affect the analyses. To this end, the results attained from the previous section by diffraction method ($\zeta = 2$) are compared with the visibility criterion. To illustrate the effect of discontinuity criterion, the J integral value has been calculated in both contour and domain forms. As depicted in Fig. 13, employing the visibility criterion, results in at least 10% difference with FEM analysis for both domain and contour J integrals. Furthermore, domain and contour forms of J have about 5% disagreement. While, diffraction method leads to at most 1% difference in J from the FEM counterpart and the contour and domain forms of J show an excellent agreement. In addition, CMOD values for different treatments of crack discontinuity are displayed in Tab. 3. Again, it can be observed that the visibility cannot appropriately model crack tip

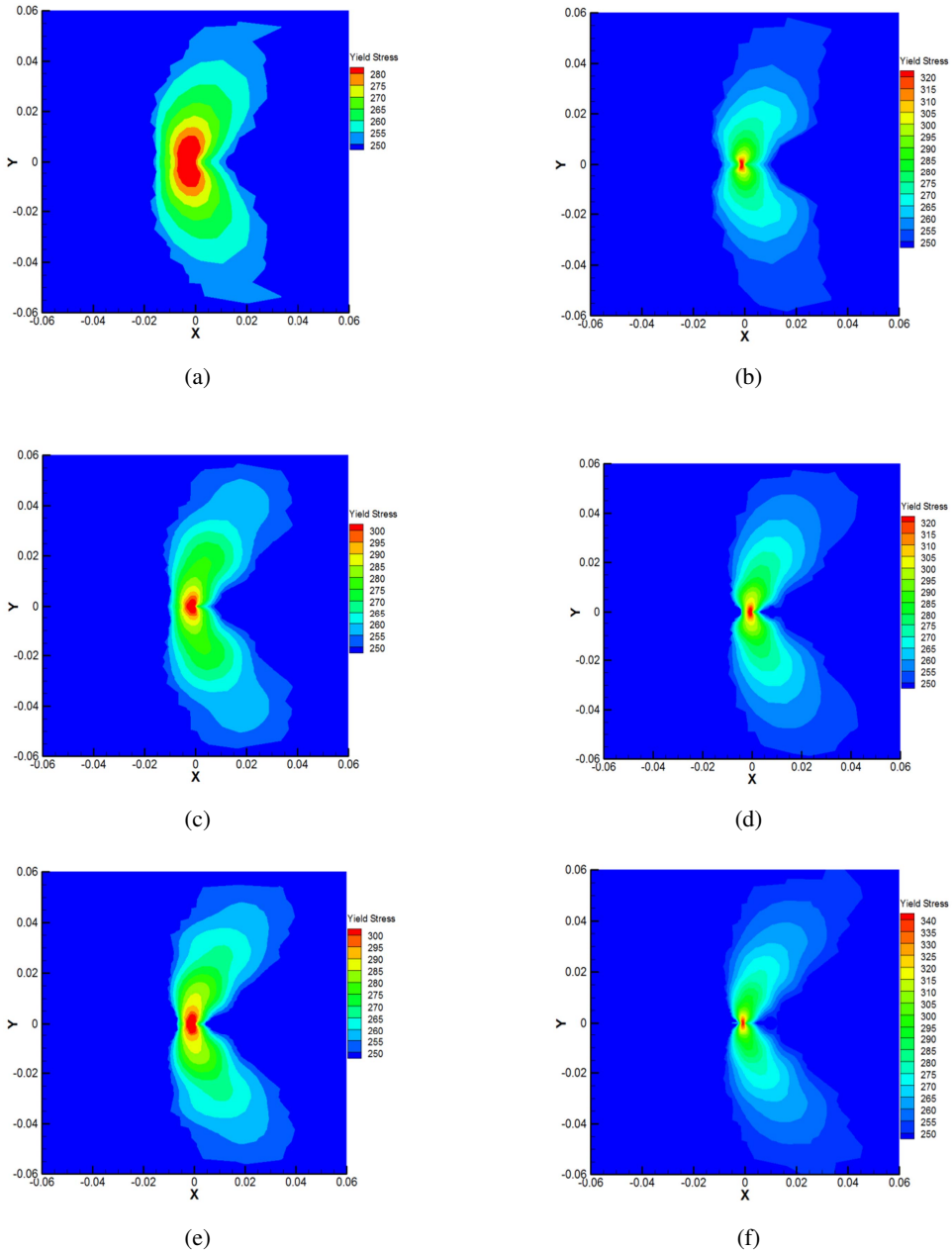


Figure 12: Contours of von Mises yield stress for monotonous and progressive arrays around the crack tip: (a) monotonous array 1 (b) progressive array 1 (c) monotonous array 2 (d) progressive array 2 (e) monotonous array 3 (f) progressive array 3

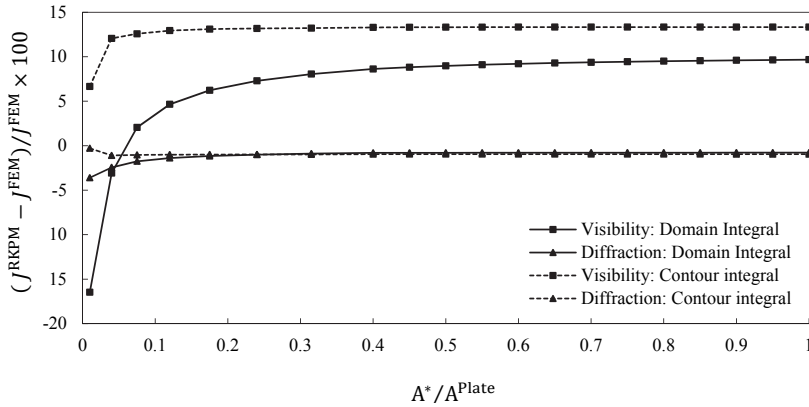


Figure 13: Contour and domain J integral difference ratios vs. relative area for the visibility and diffraction methods

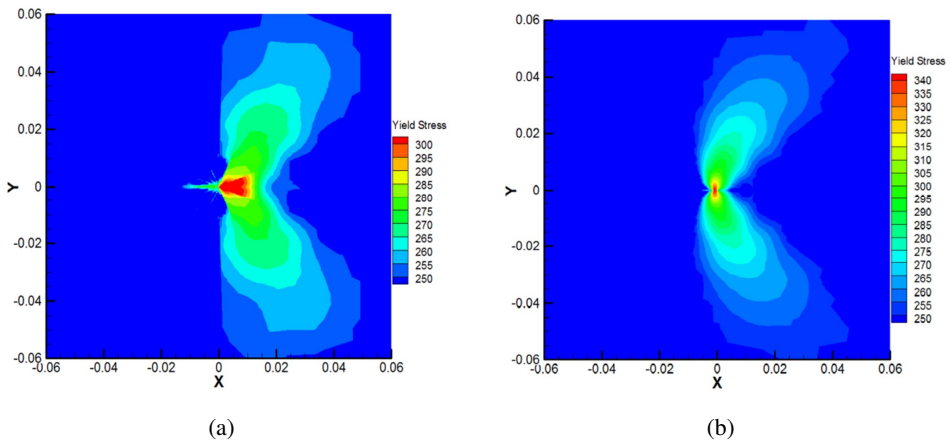


Figure 14: Contours of von Mises yield stress for different discontinuity treatments: (a) visibility criterion (b) diffraction method

fields and induces a noticeable discrepancy with FEM and diffraction results. Also, contour plots of yield stress shown in Fig. 14 at the crack tip show that the visibility is not capable of producing smooth stress field in contrast with diffraction.

Nevertheless, employing a sufficiently dense pattern of particles as a refinement at the crack tip diminishes the detrimental influence of discontinuous shape functions resulting from the visibility method, nonlinear analyses, despite of convergence

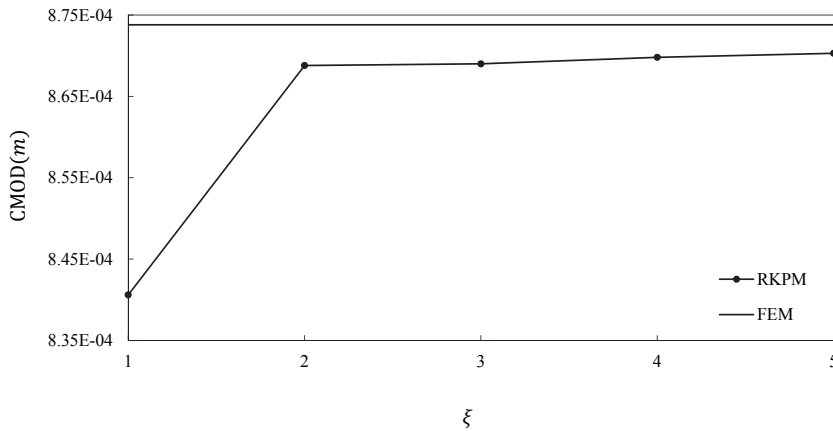


Figure 15: Domain J integral difference ratio vs relative area for different values of diffraction parameter

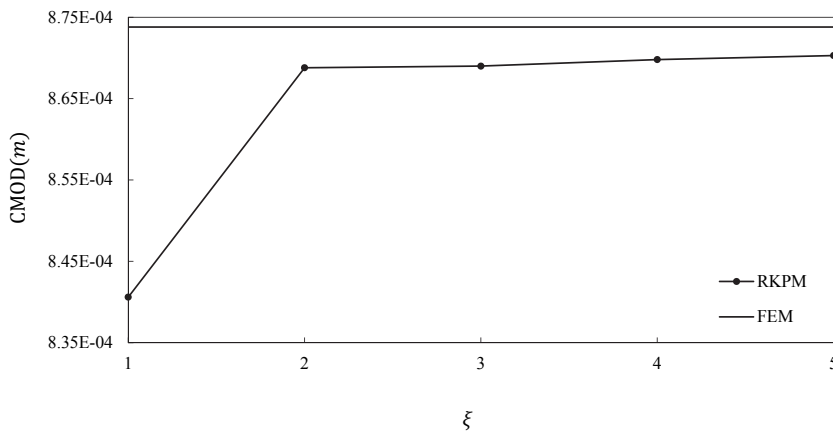


Figure 16: CMOD vs. diffraction parameter

in elastic-plastic overall procedure, exhibit a remarkable sensitivity to this kind of discontinuity and deviate from the FEM and diffraction results. This deviation is probably caused by accumulation of errors in approximating displacement increments (see Eq. (32)) by discontinuous shape functions in the vicinity of the crack tip.

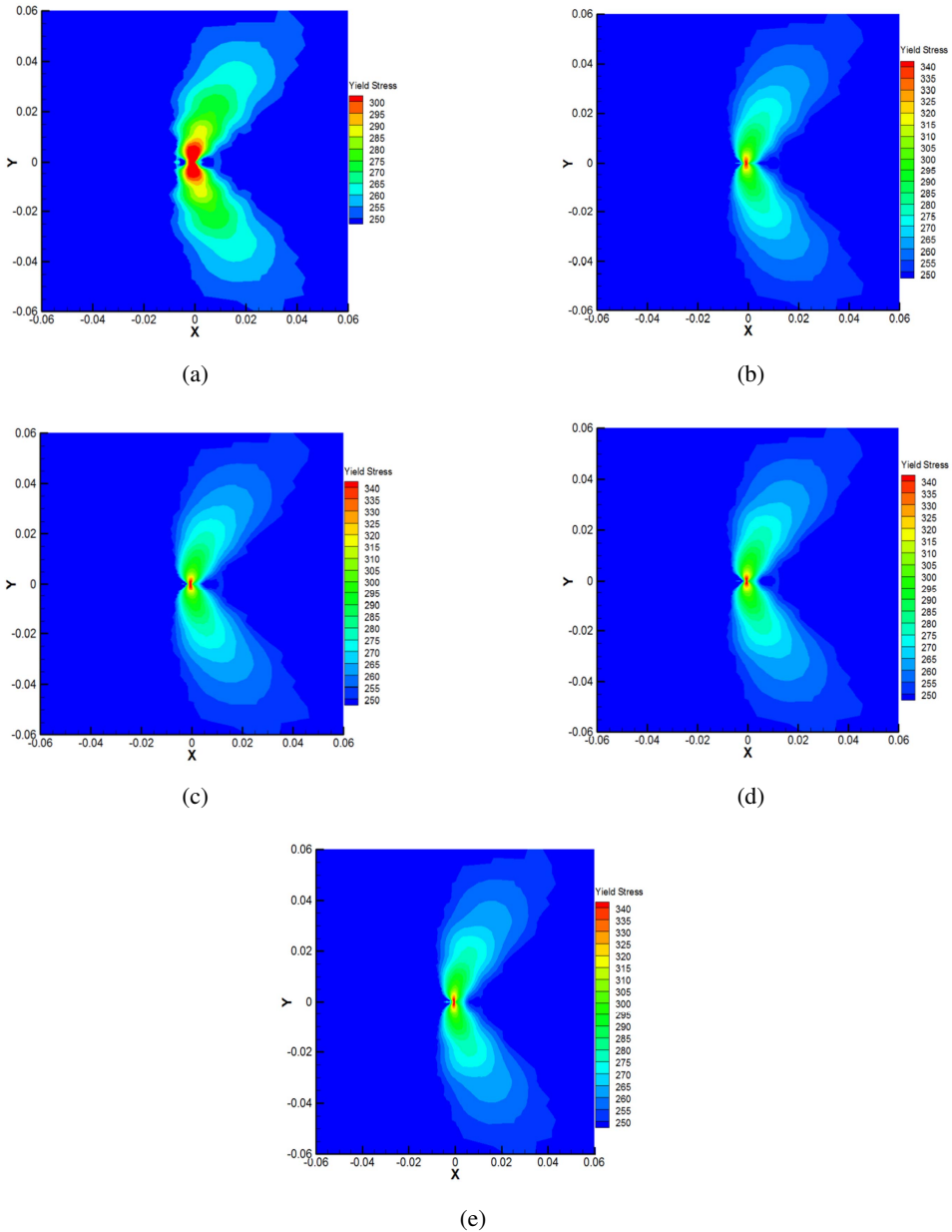


Figure 17: Contours of von Mises yield stress for different values of diffraction parameters: (a) $\zeta = 1$ (b) $\zeta = 2$ (c) $\zeta = 3$ (d) $\zeta = 4$ (e) $\zeta = 5$

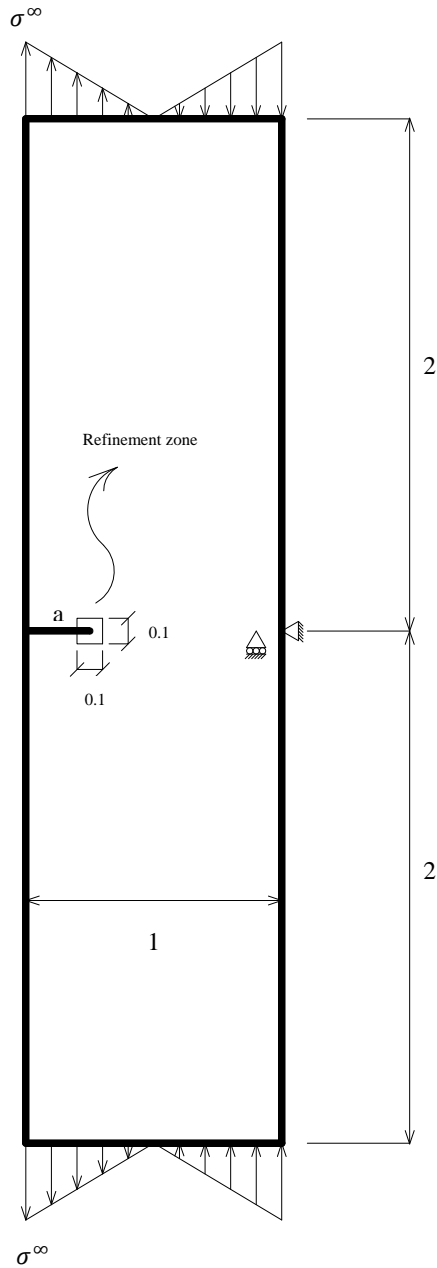
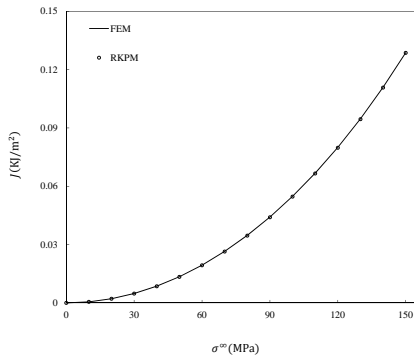
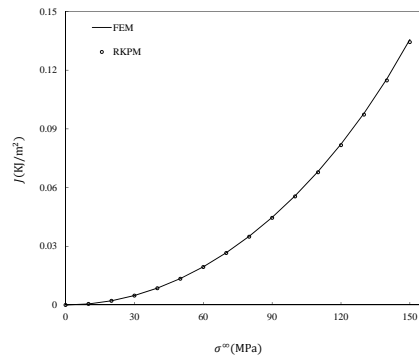


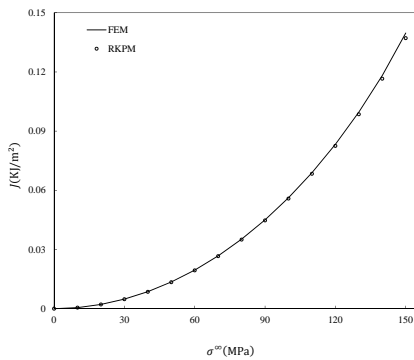
Figure 18: Edge-cracked plate under far-field bending stress



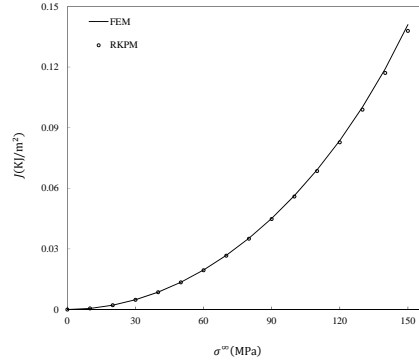
(a)



(b)



(c)



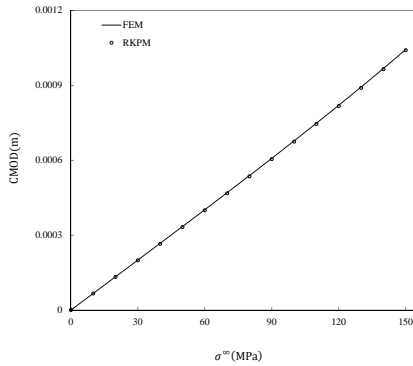
(d)

Figure 19: J integral values vs. far-field tensile stress with different hardening parameters: (a) $n=3$ (b) $n=10$ (c) $n=50$ (d) perfectly plastic

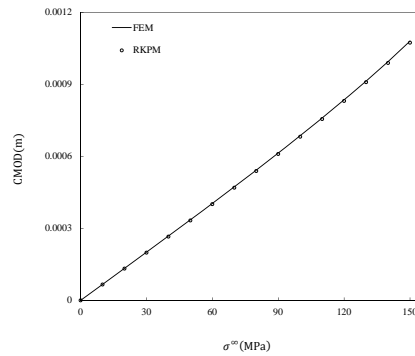
7.3 Diffraction parameter tracking

Throughout what have been examined up until now, the diffraction parameter $\zeta = 2$ has been used, which in the literature is recommended. At this point, a parameter tracking is performed to determine what ζ yields more desirable results. Hence, as preceding juxtapositions, J integral (in its domain form) and CMOD values for $\zeta = 1$ to 5 are calculated, by assuming progressive array 3, and compared with FEM ones (Figs. 15 and 16). Also, to have a better insight of stress distribution, the contours of von Mises yield stress are outlined in Fig. 17.

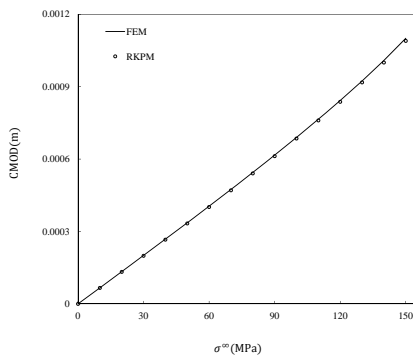
As ζ grows the breadth of the wrap-around region shrinks down, and the gradi-



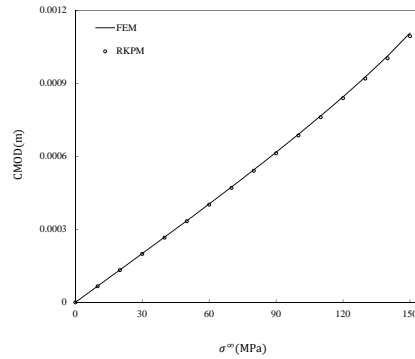
(a)



(b)



(c)



(d)

Figure 20: CMOD values vs. far-field tensile stress with different hardening parameters: (a) $n=3$ (b) $n=10$ (c) $n=50$ (d) perfectly plastic

ents of the shape functions at the crack tip intensify, and the discontinuity along the crack line is more preserved. On the other hand, if ζ assumes a relatively large quantity, the resulting shape functions in the vicinity of the crack tip tend to visibility ones where abrupt changes in shape functions deteriorate the RKPM approximation at crack tip. Considering J integral and CMOD values, and contours of von Mises yield stress, it can be concluded that $\zeta = 1$ does not yield suitable results and adopting $\zeta = 3$ or 4 lead to some improvement in results during a nonlinear analysis.

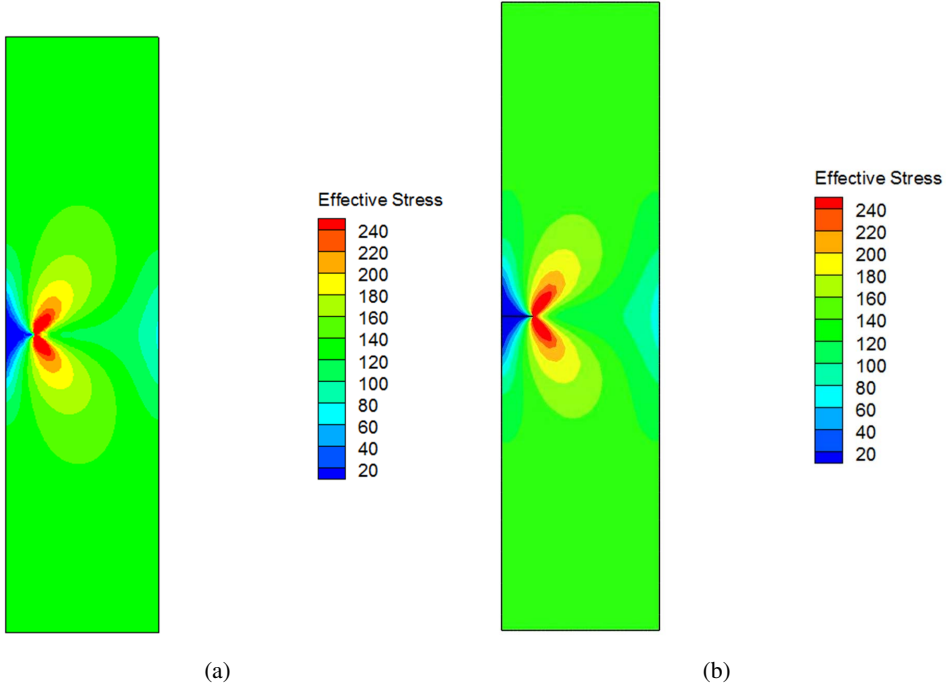
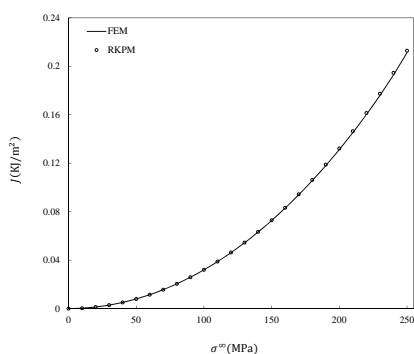


Figure 21: Contours of effective stress resulting from (a) RKPM and (b) FEM for pure tension test

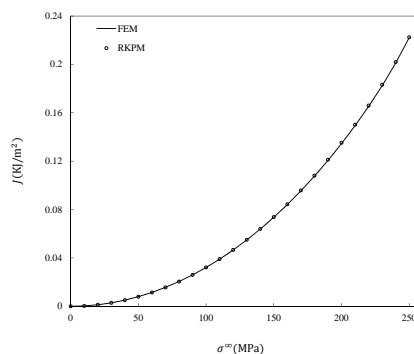
7.4 Verification tests

From what can be inferred from sections 7.1 to 7.3, by choosing progressive array 3, diffraction parameter $\zeta = 4$, and the same material properties and geometrical specifications described in 7.1, two mode (I) problems, pure tension and pure bending, are analyzed. During the tension test, ultimate far-field tensile stress $\sigma^\infty = 150\text{MPa}$, and for the bending test, ultimate far-field bending stress $\sigma^\infty = 250\text{MPa}$ (as displayed in Fig. 18) are applied. The loading increment is assumed $\Delta\sigma^\infty = 10\text{MPa}$ for both cases. To investigate the effect of hardening, parameter n , appeared in Eq. (62), takes the values 3, 10, and 50 representing high, medium, and low hardening respectively. Eventually, an elastic-perfectly plastic material behavior is simulated. For all experiments, the values of J integral and CMOD attained by RKPM and FEM are plotted together.

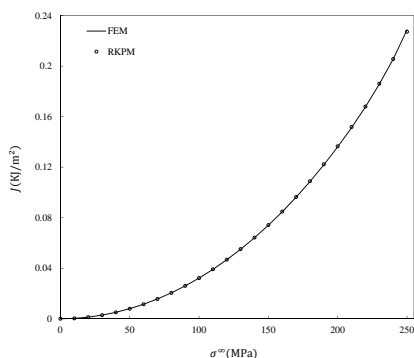
Since contained yielding condition is governing, according to Figs. 19 and 22 it is expected that for all hardening behaviors, J vs. σ^∞ diagrams would resemble a parabola closely, and also from Figs. 20 and 23, it can be concluded that there is



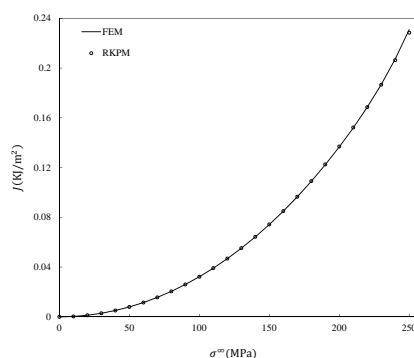
(a)



(b)



(c)



(d)

Figure 22: J integral values vs. far-field bending stress with different hardening parameters: (a) $n=3$ (b) $n=10$ (c) $n=50$ (d) perfectly plastic

an almost linear relationship between CMOD and σ^∞ . However, for low hardening and no hardening cases, i.e. $n = 50$ and elastic-perfectly plastic behaviors respectively, for high magnitudes of far-field loading, CMOD vs. ϕ^∞ diagrams show non-linear relationship, especially in the bending case. This may be explained in the way that the plastic zone created at the crack tip is so large that it acts like a plastic hinge; hence, the crack surfaces can depart from each other increasingly. The contours of effective stress σ^{eff} resulting from RKPM and FEM analyses in an elastic-perfectly plastic material for the ultimate magnitudes of loading are juxtaposed (Figs. 21 and 24).

From diagrams and contours depicted, it can be seen that the results of RKPM

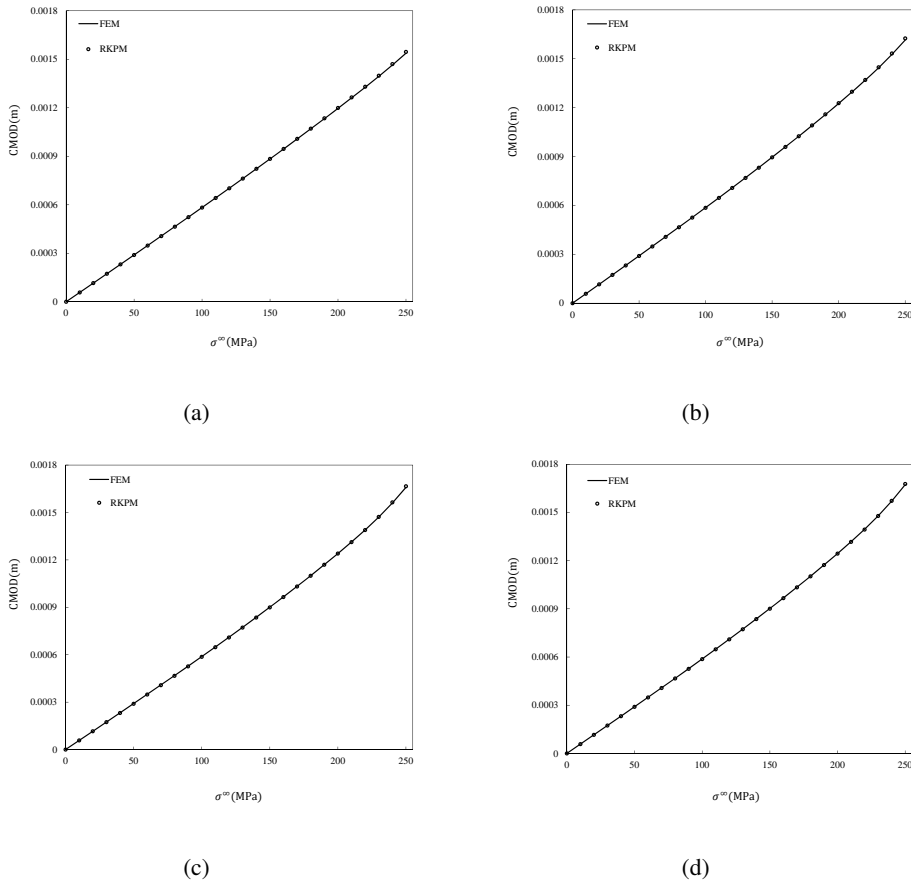


Figure 23: CMOD values vs. far-field bending stress with different hardening parameter: (a) $n=3$ (b) $n=10$ (c) $n=50$ (d) perfectly plastic

analyses are coincident with FEM ones.

8 Conclusions

For the elastic-plastic behavior, the weak form in which the essential boundary conditions are imposed by the penalty method is derived from the weighted residual method. A linearization of the obtained weak form is presented by Eq. (27). Then, nonlinear analyses for an edge-cracked plate with elastic-plastic material behavior complying modified Ramberg-Osgood relationship, which is commonly used in engineering problems to cover a wide range of material nonlinearity, were performed via RKPM. The computed values of J integral, CMOD, and contours of effective

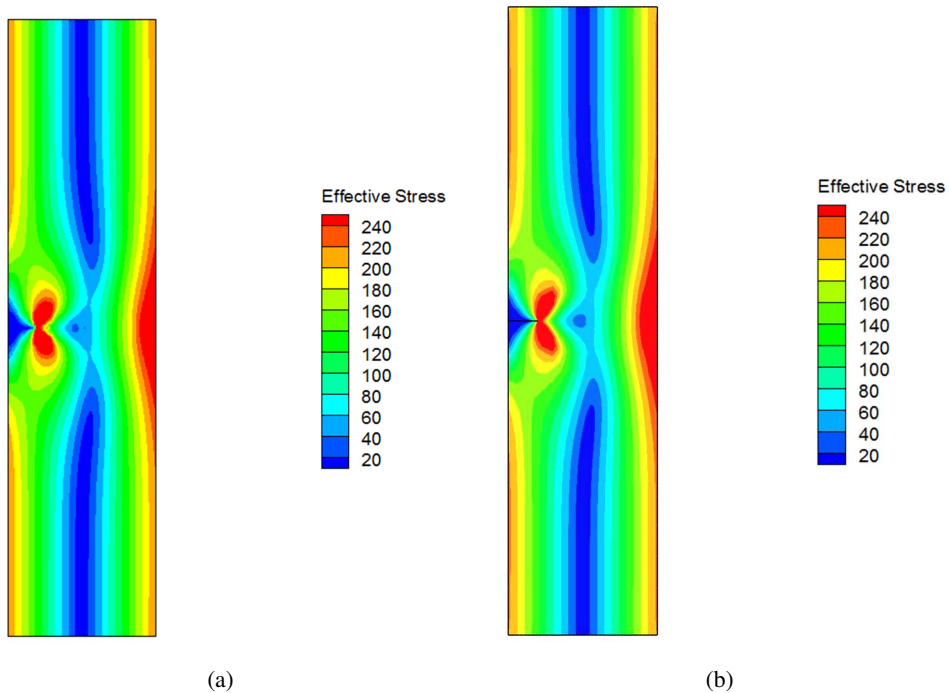


Figure 24: Contours of effective stress resulting from (a) RKPM and (b) FEM for pure bending test

stress were compared with the corresponding FEM results. Assuming arithmetic progressive arrangement of rings of particles around the crack tip in the refinement zone, instead of monotonous ones, exhibited remarkable improvement in the accuracy. To sidestep enriched basis functions to solve fracture mechanics problems, resulting in a time-consuming procedure, this economical idea can be exploited. By comparing visibility and diffraction treatments to a discontinuous domain, adopting visibility criterion, even with a dense progressive array of particles around the crack tip as a refinement, does not work accurately in EPFM problems at all. In addition, despite what was proposed previously that $\zeta = 1$ and 2 work well for the diffraction method in modeling a crack, it was observed that $\zeta = 3$ and 4 yield better results. Finally, to demonstrate the capability of RKPM in modeling EPFM, the edge-cracked plate was subjected to first, far-field pure tension and then, pure bending stresses for high, medium, low, and no hardening material behaviors. The results were in a good agreement with the ones obtained through FEM analyses.

References

- Anderson, T. L.** (1995): *Fracture mechanics*. CRC Press, Boca Raton, FL, USA.
- Atluri, S. N.** (2004): *The Meshless Local Petrov-Galerkin (MLPG) Method for Domain & Boundary Discretizations*, Tech Science Press.
- Atluri, S. N.; Kim, H. G.; Cho, J. Y.** (1999): A Critical Assessment of the Truly Meshless Local Petrov-Galerkin (MLPG) and Local Boundary Integral Equation (LBIE) Methods, *Computational Mechanics*, vol. 24, no. 5, pp. 348-372.
- Atluri, S. N.; Shen, S.** (2002): The meshless local Petrov-Galerkin (MLPG) method: A simple & less-costly alternative to the finite element and boundary element methods. *CMES: Computer Modeling in Engineering & Sciences*, vol. 3, no. 1, pp. 11-52.
- Atluri, S. N.; Zhu, T.** (1998): A new meshless local Petrov-Galerkin (MLPG) approach in computational mechanics. *Computational Mechanics*, vol. 22, pp. 117-127.
- Behzadan, A.; Shodja, H. M.; Khezri, M.** (2010): A unified approach to the mathematical analysis of generalized RKPM, gradient RKPM, and GMLS. *Computational Methods in Applied Mechanics and Engineering*. vol. 200, pp. 540-576.
- Belytschko, T.** (1997): Crack propagation by element-free Galerkin methods. *Final report; Air Force Research Grant F49620-94-0117*.
- Bakker, A.** (1984). The three-dimensional J-integral: an investigation into its use for post-yield fracture assessment. *WTHD No. 167, Laboratory for Thermal Power Engineering, Delft University of Technology, Mekelweg 2, 2628 CD, Delft*.
- Belytschko, T.; Krongauz, Y.; Organ, D.; Fleming, M.; Krysl, P.** (1996): Meshless methods: an overview and recent developments. *Computational Methods and Applied Mechanics Engineering*, vol. 139, pp. 3-47.
- Belytschko, T.; Lu, Y. Y.; Gu, L.** (1994): Element-free Galerkin methods. *International Journal for Numerical Methods in Engineering*, vol. 37, pp. 229-256.
- Budiansky, B.; Rice, J.** (1973): Conservation laws and energy release rates. *Journal of Applied Mechanics*, vol. 40, pp. 201-203.
- Cherepanov, G. P.** (1967): The propagation of cracks in a continuous medium. *Journal of Applied Mathematics and Mechanics*, vol. 31, pp. 503-512.
- De Souza Neto, E. A.; Peric, D.; Owen, D. R. J.** (2008): *Computational methods for plasticity: Theory and applications*. 1st edition UK: WILEY.
- Eshelby, J. D.** (1970). *Energy relations and the energy momentum tensor in continuum mechanics*. in *Inelastic Behavior of Solids*. Kanninen MF, et. al; McGraw Hill NY.

Hashemian, A.; Shodja, H. M. (2008a): Gradient reproducing kernel particle method. *Journal of Mechanics of Materials and Structures*, vol. 3, pp. 127-152.

Hashemian, A.; Shodja, H. M. (2008b): A meshless approach for solution of Burgers' equation. *Journal of Computational Applied Mathematics*, vol. 220, pp. 226-239.

Hutchinson, J. W. (1968): Singular behavior at the end of tensile crack in a hardening material. *Journal of Mechanics and Physics of Solids*, vol. 16, pp. 13-31.

Jin, X.; Li, G.; Aluru, N. R. (2001): On the equivalence between least-squares and kernel approximations in meshless methods. *CMES: Computer Modeling in Engineering and Sciences*, vol. 2, pp. 447-462.

Khezri, M.; Hashemian, A.; Shodja, H. M. (2009): Analysis of a crack problem via RKPM and GRKPM and a note on particle volume. *ICCEF' 09: International Conference of Computational and Experimental Engineering Science*, vol. 11, no. 4, pp. 99-108.

Krysl, P.; Belytschko, T. (1996): Element-free Galerkin: Convergence of the continuous and discontinuous shape functions. *Computer Methods in Applied Mechanics*, vol. 148, pp. 257-277.

Li, F. Z.; Shih, C.F.; Needleman, A. (1985): A comparison of methods for calculating energy release rates. *Engineering Fracture Mechanics*, vol. 21, pp. 405-421.

Li, S.; Liu, W. K. (2004): *Meshfree particle methods*. Springer Berlin Heidelberg New York.

Liu, G. R. (2003): *Mesh Free Methods: Moving beyond the finite element method*. 1st edition New York: CRC Press.

Liu, W. K.; Chen, Y. (1995): Wavelet and multiple scale reproducing kernel methods. *International Journal for Numerical Methods in Fluids*, vol. 21, pp. 901-931.

Liu, W. K.; Chen, Y.; Uras, R. A.; Chang C. T. (1996): Generalized multiple scale reproducing kernel particle methods. *Computer Methods in Applied Mechanics and Engineering*, vol. 139, pp. 91-157.

Liu, W. K.; Jun, S.; Zhang, Y. F. (1995): Reproducing Kernel Particles Methods. *International Journal for Numerical Methods in Fluids*, vol. 20, pp. 1081-1106.

Liu, W. K.; Li, S.; Belytschko, T. (1997): Moving least-square reproducing kernel methods (I) Methodology and Convergence. *Computer Methods in Applied Mechanics and Engineering*, vol. 143, pp. 113-154.

Lu, Y. Y.; Belytschko, T.; Gu, L. (1994): A new implementation of the element free Galerkin method. *Computer methods in applied mechanics and engineering*, vol. 113, pp. 397-414.

- Moran, B.; Shih, C. F.** (1987): Crack tip and associated domain integrals from momentum and energy balance. *Engineering Fracture Mechanics*, vol. 27, pp. 615-642.
- Nguyen, V. P.; Rabczuk, T.; Bordas, S.; Duflot, M.** (2008): Meshless methods: A review and computer implementation aspects. *Mathematics and Computers in Simulation*, vol. 79, pp. 763-813.
- Nikishkov, G. P.; Atluri, S. N.** (1987a): An equivalent domain integral method for computing crack-tip integral parameters in non-elastic, thermo-mechanical fracture. *Engineering Fracture Mechanics*, vol. 26, pp. 851-867.
- Nikishkov, G. P.; Atluri, S. N.** (1987b): Calculation of fracture mechanics parameters for an arbitrary three-dimensional crack, by the 'Equivalent Domain integral method'. *International Journal for Numerical Methods in Engineering*, vol. 24, pp. 1801-1827.
- Organ, D.; Fleming, M.; Terry, T.; Belytschko, T.** (1996): Continuous meshless approximations for nonconvex bodies by diffraction and transparency. *Computational Mechanics*, vol. 18, pp. 225-235.
- Owen, D. R. J.; Hinton, E.** (1980): *Finite element in plasticity: Theory and practice*. Swensea, UK: Pineridge Press Limited.
- Rao, B. N.; Rahman, S.** (2004): An enriched meshless method for non-linear fracture mechanics. *International Journal for Numerical Methods in Engineering*, vol. 59, pp. 197-223.
- Rice, J. R.** (1968): A path independent integral and the approximate analysis of strain concentration by notches and cracks. *Journal of Applied Mechanics*, vol. 35, pp. 379-386.
- Rice, J. R.; Rosengren G. F.** (1968): Plane strain deformation near a crack tip in a power hardening material. *Journal of Mechanics and Physics of Solids*, vol. 16, pp. 1-13.
- Shih, C. F.; Moran, B.; Nakamura, T.** (1986): Energy release rate along a three-dimensional crack front in a thermally stressed body. *International Journal of Fracture*, vol.30, pp. 79-102.
- Shih, C. F.; Needleman, A.** (1984): Fully plastic crack problems, Part 1: Solutions by a penalty method. *Journal of Applied Mechanics*, vol. 51, pp. 48-56.
- Shodja, H. M.; Hashemian, A.** (2007): A remedy to gradient type constraint dilemma encountered in RKPM. *Advances in Engineering Software*, vol. 38, pp. 229-243.
- Shodja, H. M.; Hashemian, A.** (2008): A numerical solution of 2D Buckley-Leverett equation via gradient reproducing kernel particle method. *CMES: Com-*

puter Modeling in Engineering and Sciences, vol. 32, no. 1, pp. 17–33.

Simha, N. K.; Fischer, F. D.; Shan, G. X.; Chen, C. R.; Kolednik, O. (2008): Jintegral and crack driving force in elastic–plastic materials. *Journal of the Mechanics and Physics of Solids*, vol. 56, pp. 2876–2895.

Yuan, H.; Brocks, W. (1991): On the J integral concept for elastic-plastic crack extension. *Nuclear Engineering and Design*, vol. 131, pp. 157-173.

Zhu, T.; Atluri S. N. (1998): A modified collocation method and a penalty formulation for enforcing the essential boundary conditions in the element free Galerkin method. *Computational Mechanics*, vol. 21, pp. 211-222.

Zhu, T.; Zhang, J.; Atluri S. N. (1998): A local boundary integral equation (LBIE) method in computational mechanics, and a meshless discretization approach. *Computational mechanics*, vol. 21, pp. 223-235.